Magnetic anisotropy in square pyramidal cobalt (II) complexes supported by a tetraazomacrocyclic ligand

Hui-Hui Cui,[a] Man-Man Ding,[b] Xiu-Du Zhang,[c] Wei Lv,[a] Yi-Quan Zhang,*[b] Xue-Tai Chen,*[a] Zhenxing Wang,*[d] Zhong-Wen Ouyang,[d] and Zi-Ling Xue[e]

[a]*State Key Laboratory of Coordination Chemistry, School of Chemistry and Chemical Engineering, Nanjing University, Nanjing 210023, China*

[b]*Jiangsu Key Laboratory for NSLSCS, School of Physical Science and Technology, Nanjing Normal University, Nanjing 210023, China*

[c]*College of Chemistry and Materials Science, Anhui Normal University, 189 Jiuhua Southern Road, Wuhu, China*

[d]*Wuhan National High Magnetic Field Center & School of Physics, Huazhong University of Science and Technology, Wuhan 430074, China*

[e]*Department of Chemistry, University of Tennessee, Knoxville, Tennessee 37996, USA.*

Electronic Supplementary Information

Table S1 Summary of the reported five-coordinate Co(II)-SIMs with molecular formulae $[(NNN)CoX_2]$[a]

Entry.	complex	CShM (4py)	CShM (3bpy)	τ_5	D (cm^{-1})	E (cm^{-1})	H_{dc}(T)	U_{eff}(K)[b]	τ_0 (s)[b]	C ($K^{-n}s^{-1}$)	n	Ref.
1	$[Co(L^{1a})Cl_2]$	1.68	5.47	0.052	/	/	0.06 /0.56	28.0/4.0	1.07×10^{-6} /7.44×10^{-2}	/	/	S1
2	$[Co(L^{1a})(NCS)_2]$	4.48	2.97	0.43	/	/	0.06 /0.56	17.0/3.0	5.85×10^{-6} /0.11	/	/	S1
3	$[Co(L^{1b})Cl_2]$	1.65	6.05	0.23	-22.2	3.53	0.15	/	/	/	/	S2
4	$[Co(L^{2a})(NCS)_2]$	1.62	6.40	0.27	-40.5	/	0.2	16	3.6×10^{-6}	/	/	S3
5	$[Co(L^{2b})(NCS)_2]$	1.67	4.65	0.034	-40.6	/	0.2	24	5.1×10^{-7}	/	/	S3
6	$[Co(L^{2c})Cl_2]$DCE	4.02	2.55	0.39	50.0	10	0.1	29	8.3×10^{-7}	/	/	S4
7	$[Co(L^{2c})Br_2]$MeCN	3.88	2.90	0.38	40.0	6	0.2	22	9.2×10^{-7}	/	/	S4
8	$[Co(L^{2c})I_2]$DCE	3.25	6.33	0.37	-26.0	7	0.2	12	7.5×10^{-6}	/	/	S4
9	$[Co(L^{2d})Cl_2]$	3.66	2.64	0.43	+45.7	0.24	0.6	/	/	/	/	S5
10	$[Co(L^{2e})Cl_2]$	3.27	2.91	0.31	+38.4	0.31	0.6	/	/	/	/	S5
11	$[Co(L^{2f})Cl_2]$	2.56	3.24	0.48	-43.9	0.26	0.6	/	/	/	/	S5
12	$[Co(L^{2g})Cl_2]$	1.83	6.13	0.089	-41.3	0.0	0.6	22.8	5.23×10^{-9}	83.2	3	S5
13	$[Co(L^{3a})Cl_2]\cdot$(MeOH)	1.74	6.08	0.27	14.5	0	0.1	19.6	5.8×10^{-5}	/	5.5	S6
14	$[Co(L^{3a})Br_2]\cdot$(MeOH)	2.16	6.93	0.23	8.4	0	0.1	8.2	3.1×10^{-5}	/	4.6	S6
15	$[Co(L^{3a})(NCS)_2]$	2.87	2.88	0.29	10.7	1.1×10^{-4}	0.1	9.7	4.6×10^{-5}	/	4.2	S6

16	$[Co(L^{3a})Cl_2].DMF$	1.70	5.00	0.42	58.4	/	0.2/0.4	33.2/37.3	13.4×10^{-8} /4.7×10^{-8}	4.27/6.10	5	S7
17	$[Co(L^{3a})Br_2].DMF$	2.10	5.40	0.017	47.0	0	0.2/0.4	21.0/33.1	5.7×10^{-7} /3.3×10^{-8}	9.31/10.3	5	S7
18	$[Co(L^{3b})(NCS)_2]$	1.37	5.50	0.30	24.7	8.22	0.15	24.61	5.87×10^{-7}	0.79	6.07	S8
19	$[Co(L^{3b})Cl_2]$	4.87	1.99	0.55	26.0	8.65	0.15	18.92	2.28×10^{-7}	14.93	5.78	S8
20	$[Co(L^{3b})Br_2]$	4.87	2.25	0.20	39.2	13.05	0.125	20.06	7.13×10^{-8}	5.37	7.44	S8
21	$[Co(L^{4a})Cl_2]$	2.08	4.14	0.10	/	/	0.35	49	1.4×10^{-8}	2618	0.8	S9
22	$[Co(L^{4a})(NCS)_2]$	4.06	3.07	0.36	48.0	/	0.4	/	/	/	/	S9
23	$[Co(L^{4a})(NCO)_2]$	5.97	4.00	0.46	30.0	/	0.2	25.3	4.5×10^{-7}	128	2.4	S9
24	$[Co(L^{4b})Cl_2]$	2.26	3.81	0.15	61,9	/	0.2	31.3	0.50×10^{-3}	/	/	S11
25	$[Co(L^{4c})Cl_2]$	1.90	5.17	0.010	153	/	0.2	13.5	1.35×10^{-7}	1.0×10^{-3}	4	S10,S11
26	$[Co(L^{4d})Cl_2]$	3.46	2.83	0.35	70.1	/	0.2	/	14.2×10^{-6}	/	/	S11
27	$[Co(L^{4e})Cl_2]$	4.10	2.67	0.41	46.8	/	0.2	40.5	2.12×10^{-3}	1.8	5	S11
28	$[CoL(L^{4f})Cl_2]$	1.88	6.95	0.19	87.5	/	0.2	/	4.67×10^{-6}	/	/	S11
29	$[Co(L^{5a})Cl_2]$	3.42	2.14	0.51	64.7	0.5	0.2	14.6	6.02×10^{-6}	277.71	1.05	S12
30	$[Co(L^{5a})Br_2]$	4.10	2.31	0.48	45	-6.3	0.2	5.59	7.22×10^{-3}	/	/	S12
31	$[Co(L^{5b})(NCS)_2]$	1.13	6.40	0.16	/	/	0.2	14.7	5.79×10^{-6}	650.9	0.32	S13
32	$[Co(L^{5b})Br_2]$	2.62	3.76	0.19	/	/	0.2	/	/	/	/	S13
33	$[Co(L^{6})(NCS)_2]$	1.44	1.93	0.46	-36.8	8.09	0.3	/	/	/	/	S14
34	$[Co(L^{7})Cl_2]\cdot CH_3OH$	4.99	2.38	0.55	17.6	2.81	/	/	/	/	/	S15
35	$[Co(L^{7})Br_2]$	1.74	6.46	0.20	30.5	4.57	0.14	/	/	0.77	6.35	S15

36	$[Co(L^{7})(NCS)_2]$	4.96	1.24	0.71	±7.98	±2.31	0.16	/	/	/	/	S15
37	$[Co(L^{8a})Cl_2]$	5.19	2.24	0.79	/	/	/	/	/	/	/	S16
38	$[Co(L^{8b})Cl_2]$	4.73 /7.27	1.72 /3.01	0.52 /0.83	/	/	/	/	/	/	/	S16

a. The ligands L^{1a}-L^{8b}, see Scheme S1; b. U_{eff} is effective barrier to the reorientation of the magnetization and τ_0 is the relaxation time at infinite temperature; c. C and n are the parameters of a power law $\tau^{-1} = CT^n$ for a Raman-like process.

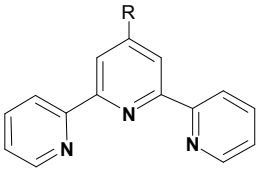

L^{1a}, R = no **1,2**
L^{1b}, R = OTf **3**

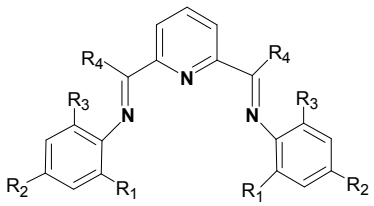

L^{2a}, $R_1 = R_3 = {}^{i}Pr$, R_2 = H, R_4 = Me, **4**
L^{2b}, $R_1 = R_3 = {}^{i}Pr$, R_2 = H, R_4 = Ph, **5**
L^{2c}, $R_1 = R_3 = R_4$ = Me, R_2 = H, **6,7, 8**
L^{2d}, $R_1 = R_2 = R_3$ = Me, R_4 = Cl, **9**
L^{2e}, $R_1 = R_3$ = Me, R_2 = H, R_4 = Cl, **10**
L^{2f}, $R_1 = R_3$ = Me, R_2 = Cl, R_4 = Cl, **11**
L^{2g}, $R_1 = R_3$ = iPr, R_2 = H, R_4 =Cl, **12**

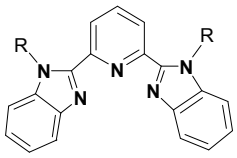

L^{3a}, R = H, **13, 14, 15, 16, 17**

L^{3b}, R = 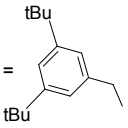 **18, 19, 20**

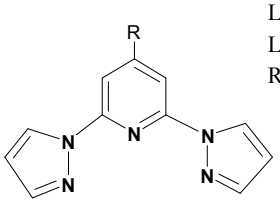

L^{4a}, R = no **21, 22, 23**
L^{4b}, R = Me **24**
R =  , n = 4, L_{4c}, **25**
n = 7, L^{4d}, **26**
n = 9, L^{4e}, **27**
n = 11, L^{4f}, **28**

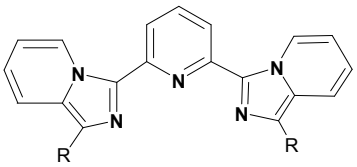

L^{5a}, R = Cl **29, 30**
L^{5b}, R = no **31, 32**

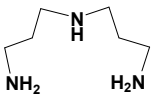

L^{6}, **33**

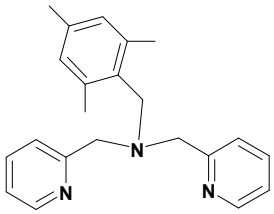

L^{7}, **34, 35, 36**

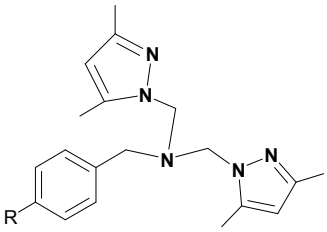

L^{8a}, R = OMe **37**
L^{8b}, R = Cl **38**

Scheme S1. Representations of the ligands in the complexes (entries 1-38) listed in Table S1.

Table S2 Summary of other reported five-coordinate Co(II)-SIMs[a]

No.	complex	CShM (4py)	CShM (3bpy)	τ_5	D (cm^{-1})	E (cm^{-1})	H_{dc}(T)	U_{eff}(K)[b]	τ_0 (s)[b]	C ($K^{-n}s^{-1}$)[c]	n[c]	Ref.
39	$[Co(L^9)(OH_2)](NO_3)_3$	5.29	0.46	0.96	/	/	0.14	18	9.6×10^{-9}	/	/	S17
40	$[Co(L^9)Cl]ClO_4$	6.20	0.89	1.03	-6.2	/	0	20.2	3.6×10^{-9}	/	/	S18-S20
41	$[Co(L^9)Br]Br$	6.56	1.27	1.03	-2.5	/	/	/	/	/	/	S20
42	$(Me_4N)[Co(L^{10})(OH_2)]\cdot DCM$	5.31	0.69	0.94	24.0	0.001	0.1	9.9	1.5×10^{-5}	0.008	7.2	S19
43	$[Co(L^{11a})Cl](BPh_4)$	4.23/ 4.86	1.06/ 0.87	0.83/ 0.91	-19.9	1.5	0.2	46	2.1×10^{-11}	/	/	S21
44	$[Co(L^{11a})Cl](BPh_4)$	4.23/ 4.86	1.06/ 0.87	0.83/ 0.91	-19.90	/	0.2	30.6/ 46.9	1.5×10^{-8}/ 1.6×10^{-11}	0.5/17.0	5	S21,S22
45	$[Co(L^{11a})Br](BPh_4)$	5.12/ 5.65	0.88/ 0.97	0.88/ 0.94	-20.0	2.0	0.2	37.8	6.4×10^{-9}	1.12	5	S22
46	$[Co(L^{11b})Br](ClO_4)$	4.81/ 5.18	1.06/ 0.90	0.87/ 0.93	-20.20	/	0.3	43.9	2.9×10^{-9}	4.10	5	S22,S23
47	$[Co(L^{11b})Cl]ClO_4$	5.66	0.66	1.00	-21.4	0.24	0.3	/	/	/	/	S23
48	$[Co(L^{11b})Br]ClO_4$	4.81/ 5.18	1.06/ 0.90	0.87/ 0.93	-20.2	0.80/2.00	0.3	30.2	4.6×10^{-8}	/	/	S23
49	$[Co(L^{11b})NCS]ClO_4$	5.20	0.61	1.04	-11.0	0	0.16	28.7	2.0×10^{-9}	/	/	S23
50	$[Co(L^{12})N_3]ClO_4\cdot 3CH_3CN$	6.20	1.63	1.00	-10.7	-2.35	0.3	28.3	1.6×10^{-8}	/	/	S24
51	$[Co(L^{12})Cl]\cdot(ClO_4)\cdot(MeCN)_2\cdot(H_2O)$	7.24	2.27	1.06	-7.5	0.4	0.1	11.6	3.5×10^{-6}	/	/	S25
52	$[Co(L^{12})Br]\cdot ClO_4$	7.83	2.42	1.10	-4.3	0.03	0.1	7.1	2.1×10^{-6}	/	/	S25

53	$[Co(L^{13})Cl]\cdot ClO_4$	6.10/ 6.57	1.88/ 1.84	0.95/ 1.00	-10.1	1.8	0.1	17.2	7.2×10^{-6}	/	/	S25
54	$[Co(L^{13})Br]\cdot ClO_4$	6.68/ 7.16	2.30/ 2.34	0.96/ 1.00	-7.8	2.1	0.1	12.5	5.8×10^{-6}	/	/	S25
55	$[Co(L^{13})\ (CH_3CN)](BF_4)_2\cdot CH_3CN$	5.74	0.98	0.99	9.66	0.26	0.1	21.5	1.7×10^{-8}	/	/	S26
56	$[Co(L^{13})Cl]Cl\cdot 2.4H_2O$	7.05/ 6.80/ 6.34	1.68/ 1.70/ 1.77	1.01/ 1.04/ 1.01	-6.95	-1.78	/	/	/	/	/	S26
57	$[Co(L^{13})Cl]Cl$	6.85	1.81	1.07	-8.49	0	0.04	21.8	2.98×10^{-8}		/	S26
58	$[Co(L^{13})Br]Br\cdot 2.0H_2O$	7.49/ 6.80/ 7.25	2.12/ 2.15/ 2.14	1.01/ 1.02/ 1.04	-6.30	1.59	/	/	/	/	/	S26
59	$[Co(L^{13})Br]Br$	7.11	2.28	1.07	-7.18	0	0.16	17.6	8.06×10^{-8}	/	/	S26
60	$[Co(L^{13})I]I$	8.18/ 7.48	3.24/ 3.09	0.99/ 1.02	-7.53	1	/	/	/	/	/	S26
61	$[Co(L^{14})(N_3)]Cl_4$	6.03	0.71	1.05	-7.10	/	0.05	21.5	5×10^{-9}	/	/	S27
62	$[Co^{II}Co^{III}_2(\mu_3\text{-}OH)(\mu\text{-}pz)_4(L^{15})_3]\cdot$ 2MeCN	5.55	0.33	0.89	23.85	4.04	0.1	/	/	2.3	6.6	S28
63	$[CoCl_3(L^{16})(HL^{15})]$	5.39	0.02	1.00	44.5	0	0.25	/	/	0.2	5.7	S29
64	$[(L^{17})_2Co_4Li_8(H_2O)_{12}]$	2.94	0.83	0.69	27.9	-6.3	0.07	21.5	6.2x10−8			S30
65	$[Co(L^{18})(DMSO)Cl_2]$	2.49	2.53	0.54	-17.0	-4.08	0.1	10.4	5.69×10^{-9}	/	/	S31
66	$[Co(L^{19})(H_2O)_2]$	5.86	4.79	0.56	16.0	2	0.15	/	/	/	/	S32
67	$[Co(L^{19})(L^{20})_{0.5}(H_2O)]\cdot H_2O$	3.62	2.26	0.64	59.0	7	0.3	8.6	1.7×10^{-5}	/	/	S32
68	$[Co(L^{21})Cl]ClO_4$	1.14	3.31	0.33	46.4	10.1	0.1	/	/	/	5.8	S33

69	$[Co(L^{21})Br]ClO_4$	1.41	3.29	0.35	40.7	9.3	0.1	/	/	/	5.3	S33
70	$[Co(L^{22})_2Cl]\cdot ClO_4$	1.37	5.30	0.15	48.5	0.76	0.2	40.3	5.8×10^{-6}	/	4.3	S34
71	$[Co^{III}(N_3)_2(L^{23a})(\mu_{1,1}\text{-}N_3)Co^{II}(N_3)]\cdot$ MeOH	1.91	3.32	0.38	38.7	/	0.4	/	/	/	/	S35
72	$[Co^{III}(N_3)_2(L^{23b})(\mu_{1,1}\text{-}N_3)Co^{II}(N_3)]\cdot$ MeOH	1.87	3.40	0.36	45.7	/	0.4	/	/	/	/	S35
73	$[Co(L^{24})Cl](BF_4)$	0.56	3.04	0.27	45.1	9.9	0.2	7.3	2.7×10^{-6}	/	/	S36
74	$[Co(L^{25})Cl](ClO_4)$ (MeCN)	0.85	5.93	0.0062	52.3	10.1	0.2	18.4	3.2×10^{-6}	0.53	4.8	S36
75	$[Co(12\text{-}TMC)(CH_3CN)](BF_4)_2$	0.23	5.54	0.00	/	/	0.25	/	/	8.05	4.6	S37
76	$[Co(12\text{-}TMC)(CH_3CN)](PF_6)_2$	0.04	5.46	0.033	/	/	0.25	/	/	54.33	4	S37
77	$[Co(12\text{-}TMC)(NCO)][B(C_6H_5)_4]$	0.44	5.66	0.012	/	/	0.1	33.3	1.17×10^{-9}	6.57	5.5	S38
78	$[Co(12\text{-}TMC)Cl][B(C_6H_5)_4]$ (**1**)	0.76/ 0.76	5.62/ 5.64	0.027/ 0.023	37.76	0.52	0.08	11.38	4.86×10^{-8}	31.61	7.5	This work
79	$[Co(12\text{-}TMC)Br][B(C_6H_5)_4]$ (**2**)	1.12/ 1.08	5.98/ 5.86	0.019/ 0.024	37.10	-0.18	0.1	13.52	5.02×10^{-9}	29.83	8.6	This work

b. The ligands L^9-L^{24}, see Scheme S2; b. U_{eff} is effective barrier to the reorientation of the magnetization and τ_0 is the relaxation time at infinite temperature; c. C and n are the parameters of a power law $\tau^{-1} = CT^n$ for a Raman-like process.

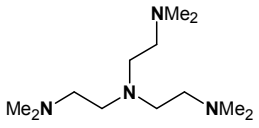

L^{9}, **39, 40, 41**

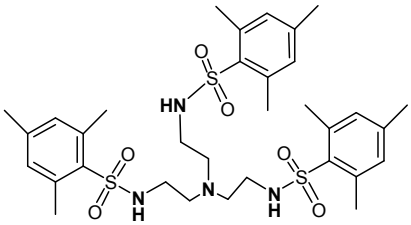

L^{10}, **42**

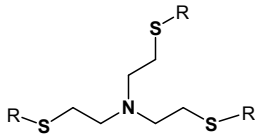

L^{11a}, R = ^{i}Pr **43 - 45**
L^{11b}, R = ^{t}Bu **46 - 49**

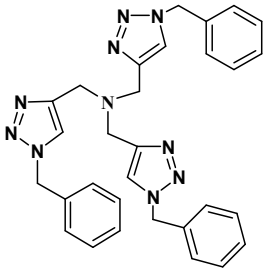

L^{12}, **50 - 52**

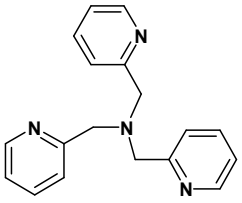

L^{13}, **53 - 60**

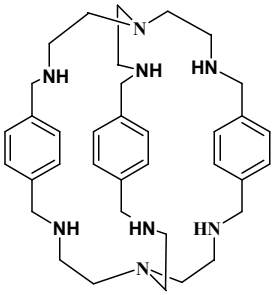

L^{14}, **61**

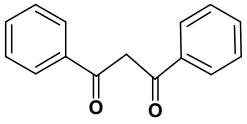

HL^{15}, **62**

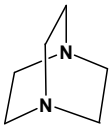

L^{16}, **63**

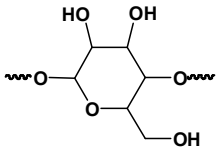

L^{17}, **64**

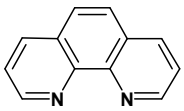

L^{18}, **65**

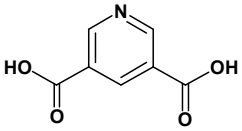

H_2L^{19}, **66**

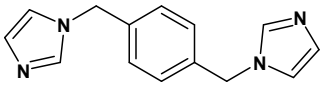

L^{20}, **67**

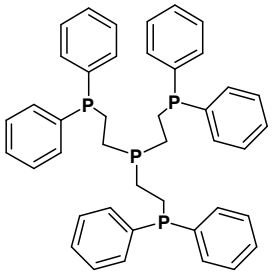

L^{21}, **68, 69**

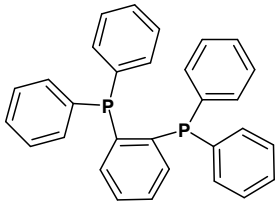

L^{22}, **70**

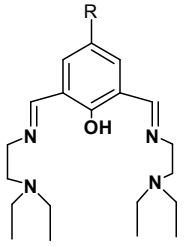

L^{23a}, R = Me **71**
L^{23b}, R = Et **72**

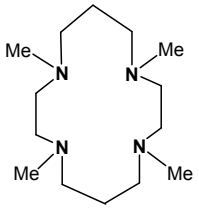

L^{24}, **73**

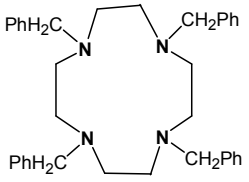

L^{25}, **74**

Scheme S2. Representations of the ligands in the complexes (entries 39-74) listed in Table S2.

Table S3 Summary of crystal data and refinement for **1** and **2**.

	1	**2**
Molecular formula	$C_{36}H_{48}BCoN_4Cl$	$C_{36}H_{48}BCoN_4Br$
CCDC no	1827493	1827494
Formula weight	641.97	686.43
Temperature	155(2) K	155(2) K
Crystal system	Monoclinic	Monoclinic
Space group	$P\ 2_1/c$	$P\ 2_1/c$
a / Å	20.999(4)	20.9569(16)
b / Å	10.347(2)	10.4803(8)
c / Å	30.920(6)	31.079(2)
α (°)	90	90
β (°)	90.724(3)	90.093(2)
γ (°)	90	90
V / Å^3	6711(2)	6821.6(9)
Z	8	8
D_{calc}, g/cm^3	1.271	1.337
μ / mm^{-1}	0.622	1.705
F (000)	2728	2872
θ range [°]	2.19/25.72	2.28/27.36
Reflns collected	57712	47519
R_{int}	0.0889	0.0796
Indep. reflns	14835	12027
Refns obs.[$I > 2\sigma(I)$]	10977	8776
Data/restr./paras	14835/0/783	12027/0/783
Goodness-of-fit on F^2	1.050	1.047
R_1, wR_2 [$I > 2\sigma(I)$][a]	0.0475/0.1072	0.0660/0.1617
R_1, wR_2 [all data][a]	0.0732/0.1186	0.0980/0.1759

[a] $wR_2 = [\Sigma[w(F_o^2 - F_c^2)^2]/\Sigma[w(Fo^2)^2]]^{1/2}$, $R_1 = \Sigma||F_o| - |F_c||/\Sigma|F_o|$.

Table S4 Selected bond lengths (Å) and angles (deg) for **1**-**2**

1a		**1b**	
Co1-N1	2.171(2)	Co2-N5	2.1464(19)
Co1-N2	2.1315(19)	Co2-N6	2.1574(19)
Co1-N3	2.163(2)	Co2-N7	2.1591(19)
Co1-N4	2.152(2)	Co2-N8	2.164(2)
Co1-Cl1	2.2425(8)	Co2-Cl2	2.2267(7)
N1-Co1-N2	81.84(7)	N5-Co2-N6	81.13(7)
N1-Co1-N3	136.78(8)	N5-Co2-N7	136.47(7)
N1-Co1-N4	81.19(8)	N5-Co2-N8	82.44(7)
N2-Co1-N3	82.04(8)	N6-Co2-N7	82.15(7)
N2-Co1-N4	135.18(8)	N6-Co2-N8	135.14(7)
N3-Co1-N4	82.66(9)	N7-Co2-N8	81.74(7)

2a		**2b**	
Co1-N1	2.137(4)	Co2-N5	2.154(4)
Co1-N2	2.179(4)	Co2-N6	2.162(4)
Co1-N3	2.149(4)	Co2-N7	2.151(4)
Co1-N4	2.166(4)	Co2-N8	2.174(4)
Co1-Br1	2.4017(10)	Co2-Br2	2.3641(8)
N1-Co1-N2	81.35(15)	N5-Co2-N6	82.32(15)
N1-Co1-N3	135.26(18)	N5-Co2-N7	136.29(14)
N1-Co1-N4	82.62(15)	N5-Co2-N8	81.79(15)
N2-Co1-N3	81.23(16)	N6-Co2-N7	82.32(15)
N2-Co1-N4	136.40(17)	N6-Co2-N8	134.87(15)
N3-Co1-N4	82.31(17)	N7-Co2-N8	82.25(16)

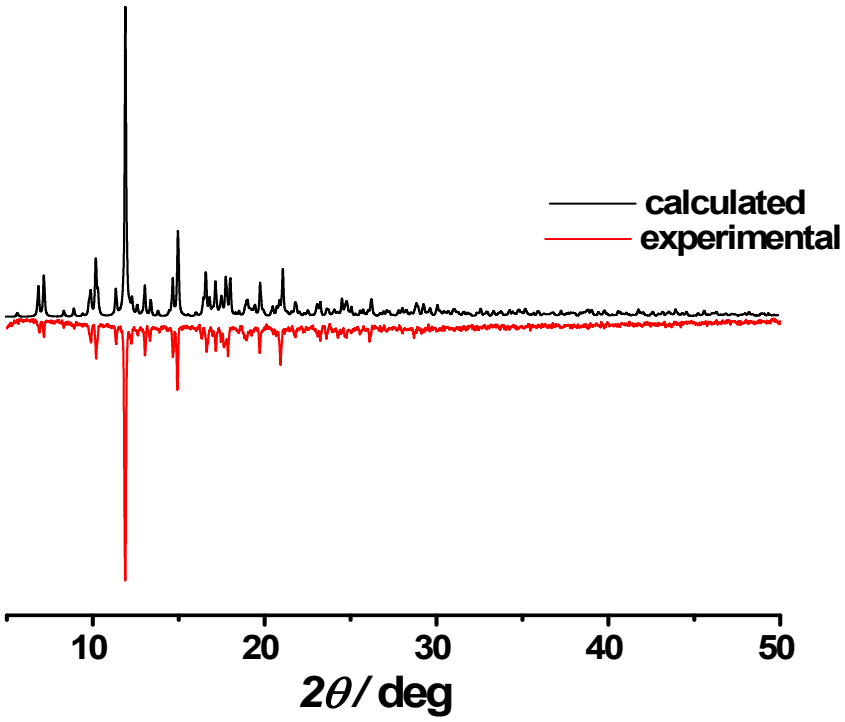

Fig. S1 XRD patterns for complex **1**.

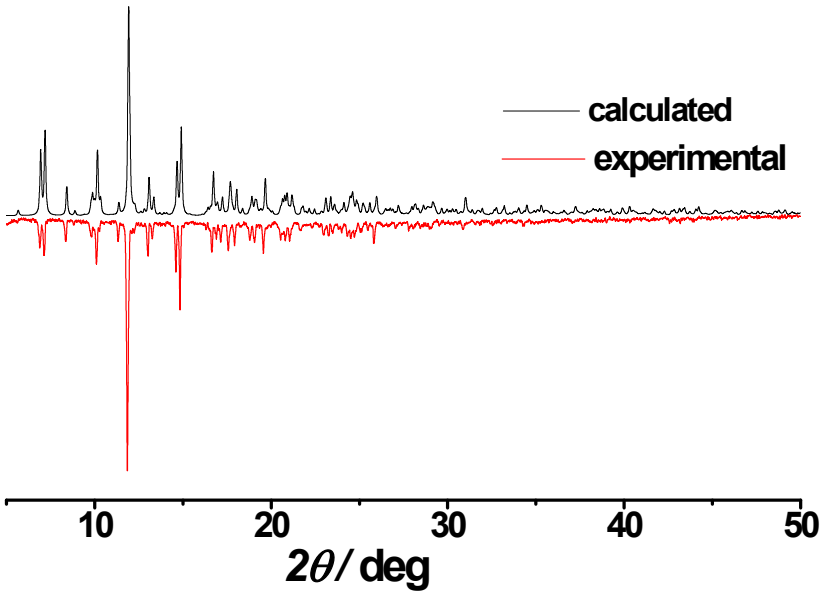

Fig. S2 XRD patterns for complex **2**.

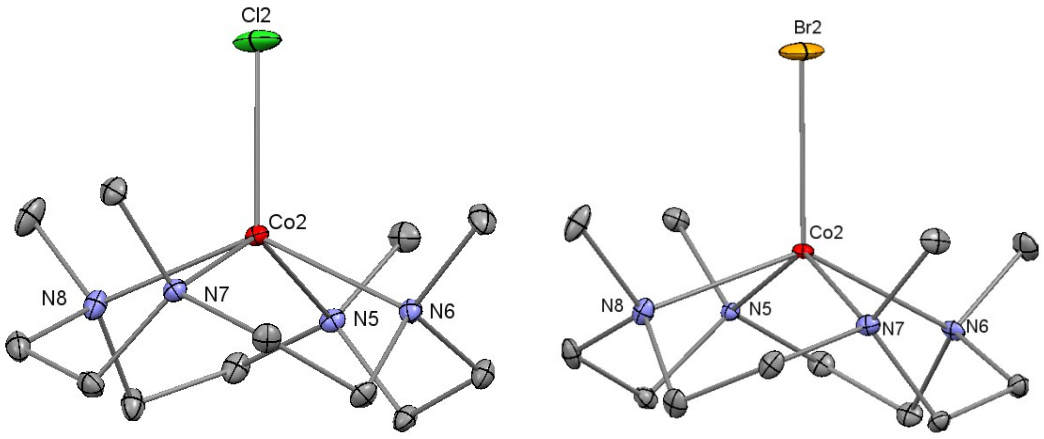

(a) **(b)**

Fig. S3 Structure of the anion of (a) **1b** and (b) **2b**. Red, blue, green, orange and gray spheres represent Co, N, Cl, Br and C atoms. H atoms are omitted for clarity.

Table S5 The results of the continuous shape measure (CShM) analyses of **1-2** by SHAPE software.[S39]

CShM value		**1a**	**1b**	**2a**	**2b**
Five-vertex	Pentagon	33.413	32.657	33.722	33.446
	Vacant octahedron	4.607	4.583	5.341	5.235
	Trigonal bipyramid	5.624	5.640	5.983	5.857
	Spherical square pyramid	0.759	0.760	1.124	1.081
	Johnson trigonal bipyramid	9.495	9.669	10.190	10.242

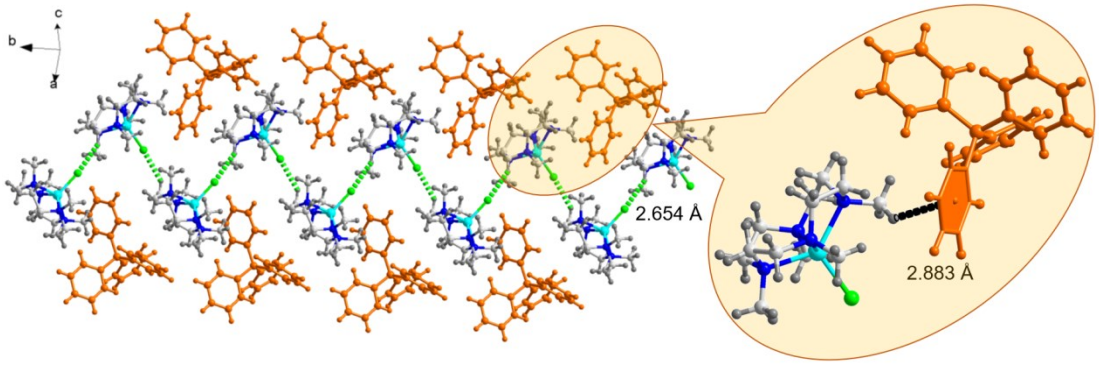

(a)

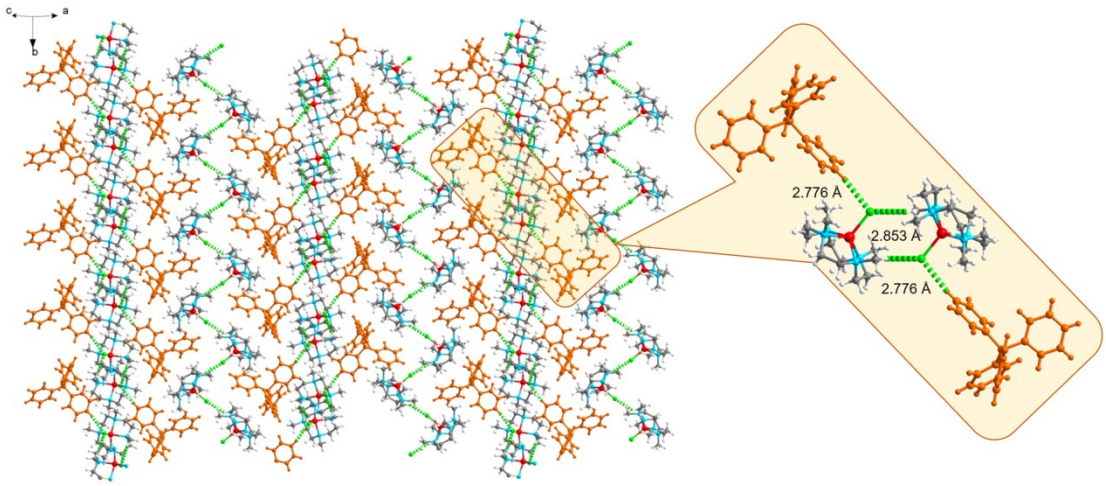

(b)

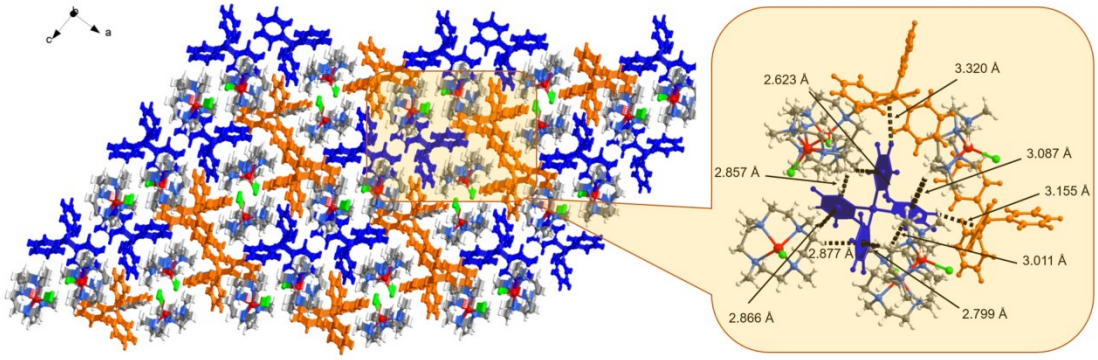

(c)

Fig. S4 The weak interactions in the crystal structure of complex **1**: (a) The one-dimensional chain of molecule **1b** (containing Co2); (b) two-dimensional sheet formed from one-dimensional chain; (c) Three-dimensional structure.

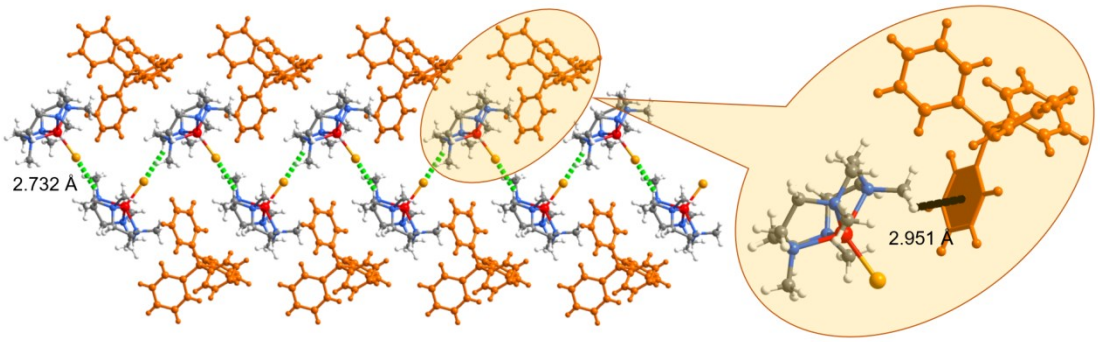

(a)

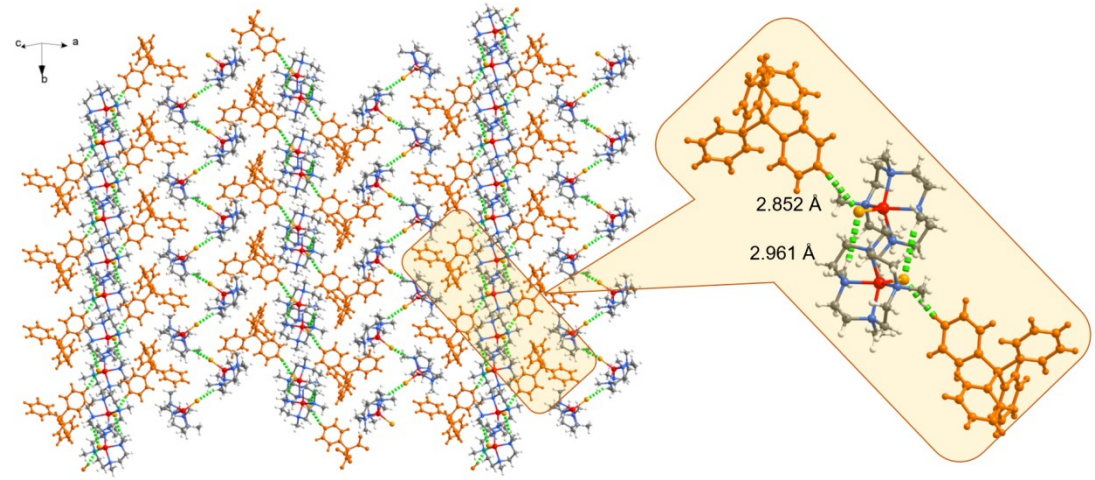

(b)

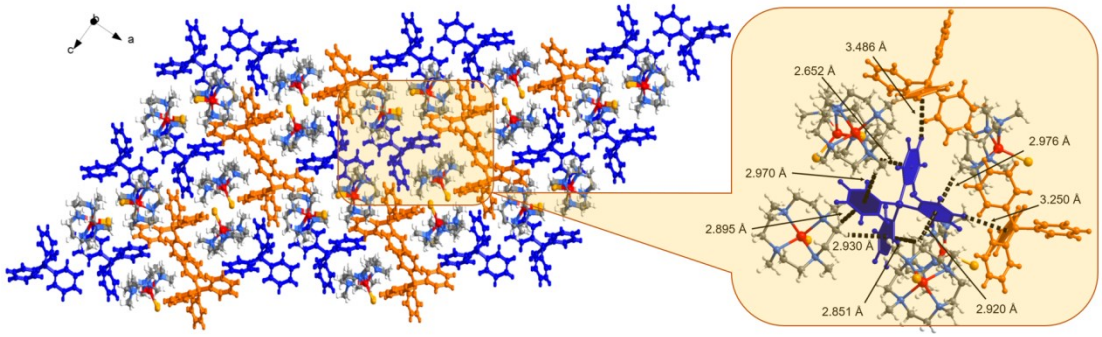

(c)

Fig. S5 The weak interactions in the crystal structure of complex **2**: (a) The one-dimensional chain of molecule **2b** (containing Co2); (b) two-dimensional structure formed from one-dimensional chain; (c) Three-dimensional structure.

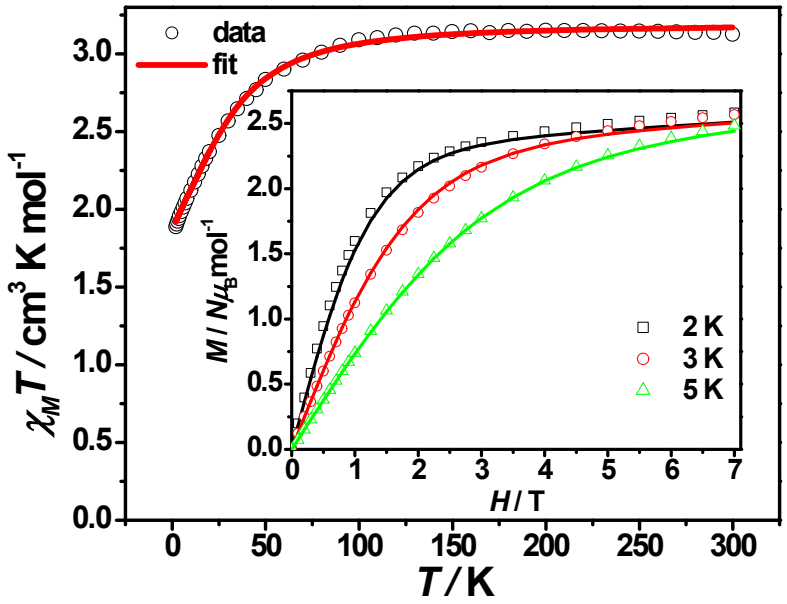

Fig. S6 Variable-temperature dc susceptibility data of **2** under 0.10 T applied dc field. Inset: field dependence of the magnetization below 5 K for **2**. Solid lines are fits to the data with the program *PHI*.[S40]

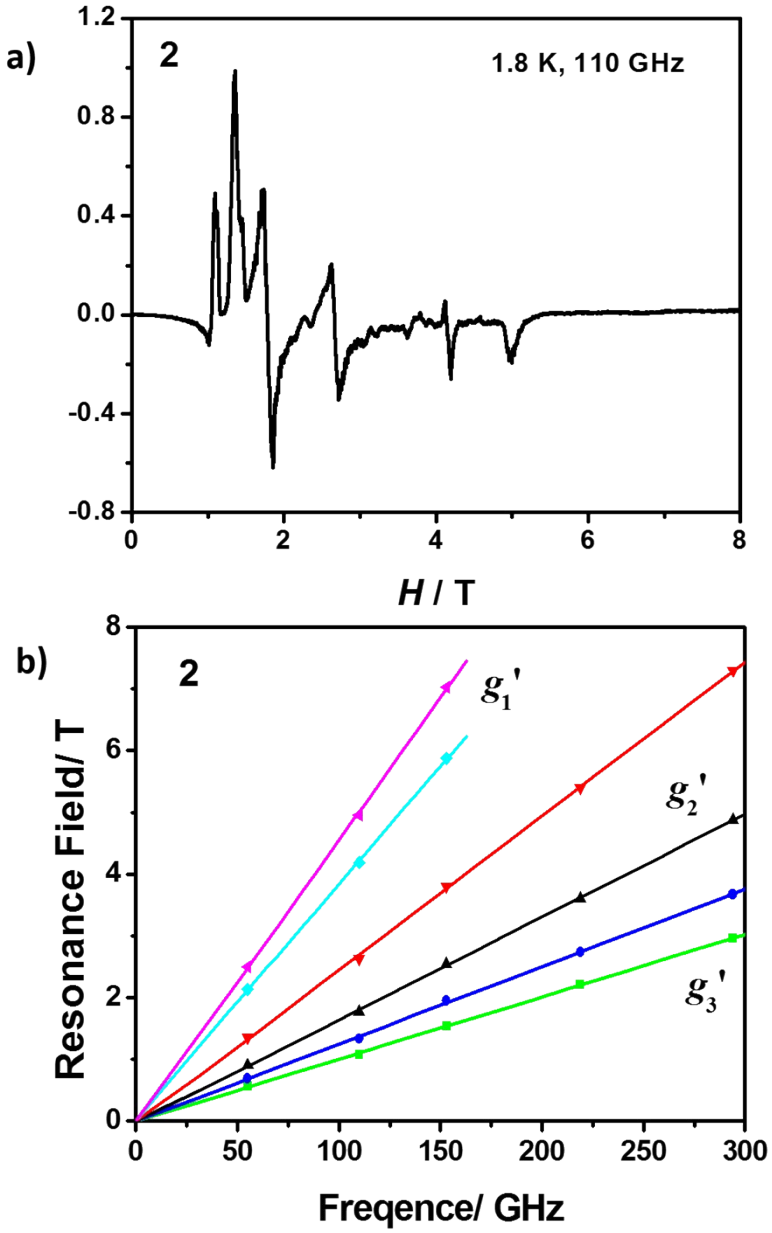

Fig. S7 a) Representative HFEPR spectra of **2** at 1.8 K; b) Resonance field vs. microwave frequency for EPR transitions for **2**. The solid lines are for eye guide.

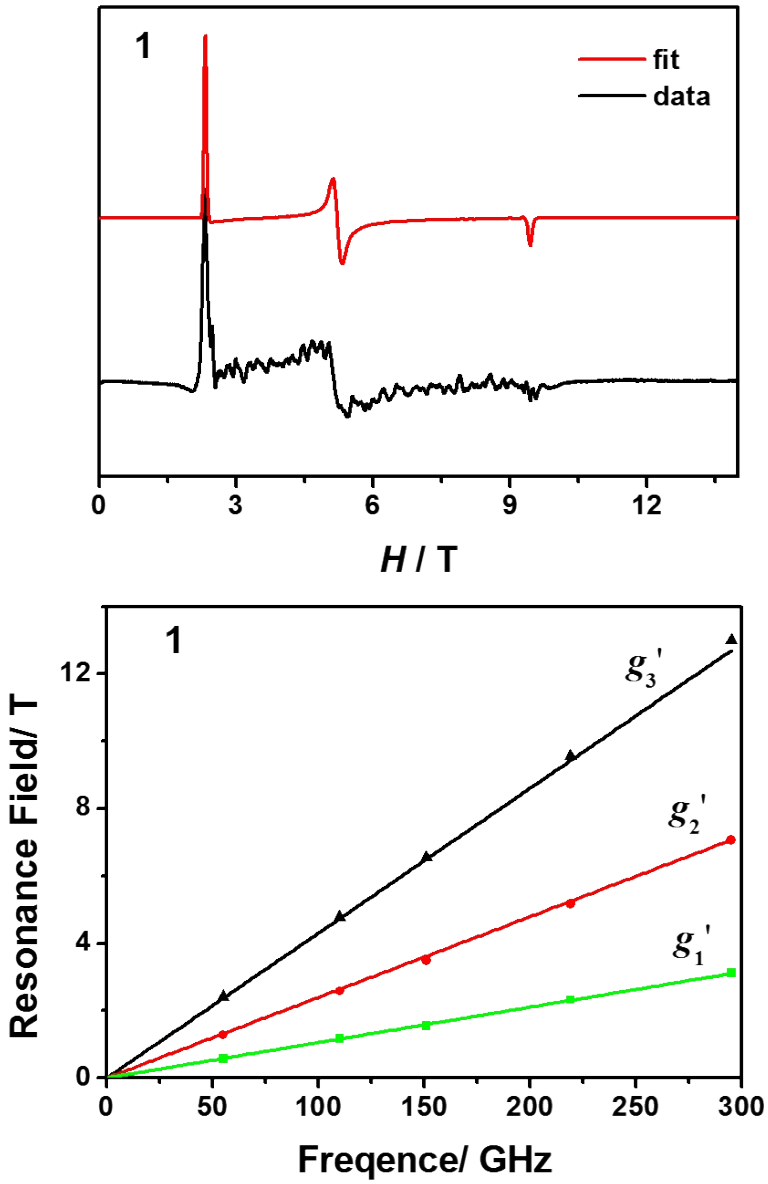

Fig. S8 a) Representative HFEPR spectrum of **1** at 1.8 K (black) with the simulation considering an effective spin S_{eff}= 1/2 at low temperature; b) Resonance field vs. microwave frequency for EPR transitions for **1** and the simlations considering an effective spin S_{eff} = 1/2.

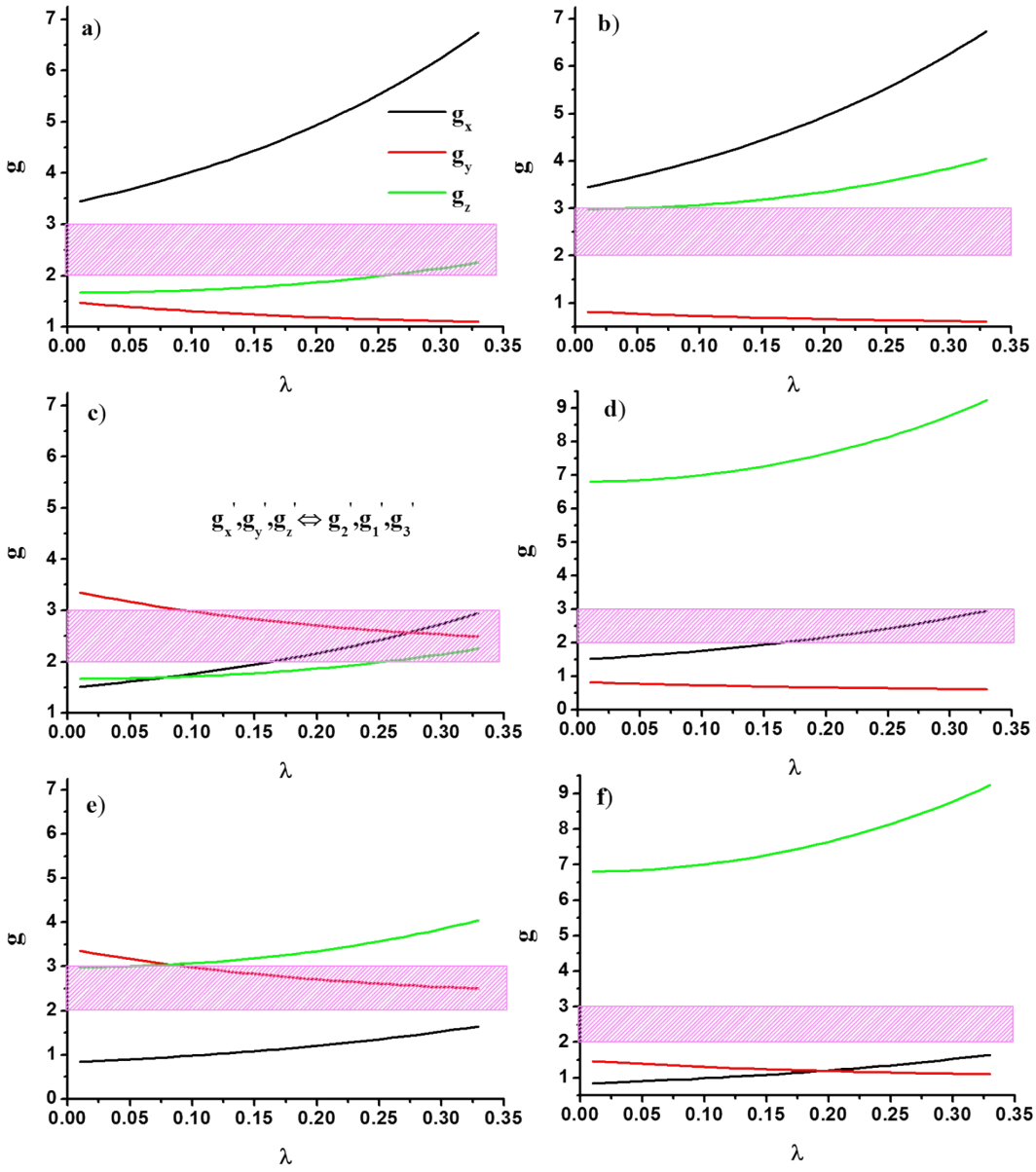

Fig. S9 Principal *g* values (*gx*: red, *gy*: green, *gz*: blue) as function of λ for all possible assignments (g_x', g_y', g_z')↔(a) - (g_1', g_2', g_3'), (b) - (g_1', g_3', g_2'), (c) - (g_2', g_1', g_3'), (d) - (g_2', g_3', g_1'), (e) - (g_3', g_1', g_2'), (f) - (g_3', g_2', g_1'). The region of realistic g values between 2 and 3 is indicated by a pink bar.

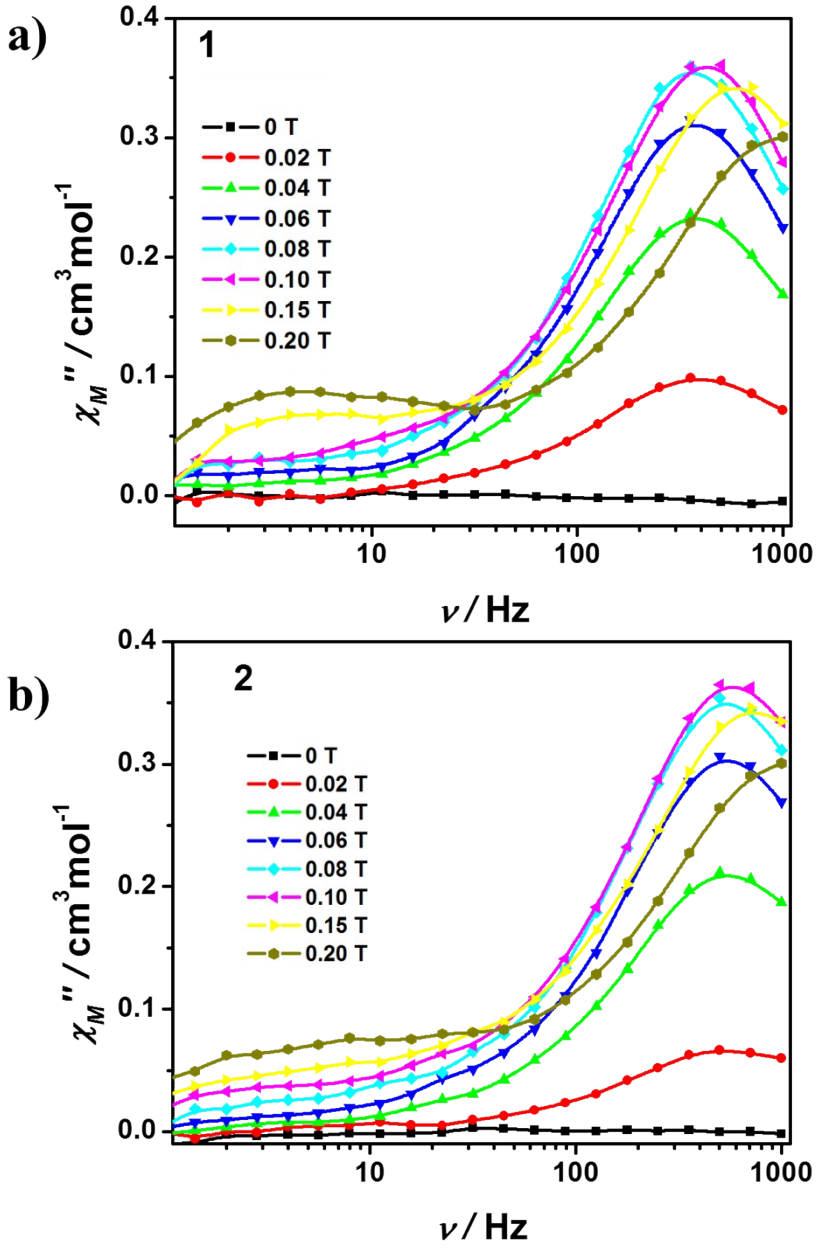

Fig. S10 Frequency dependence of out-of-phase ac susceptibility (χ_M'') at 1.8 K under the different applied static fields from 0 to 0.20 T for a) **1** and b) **2**. The solid lines are for eye guide.

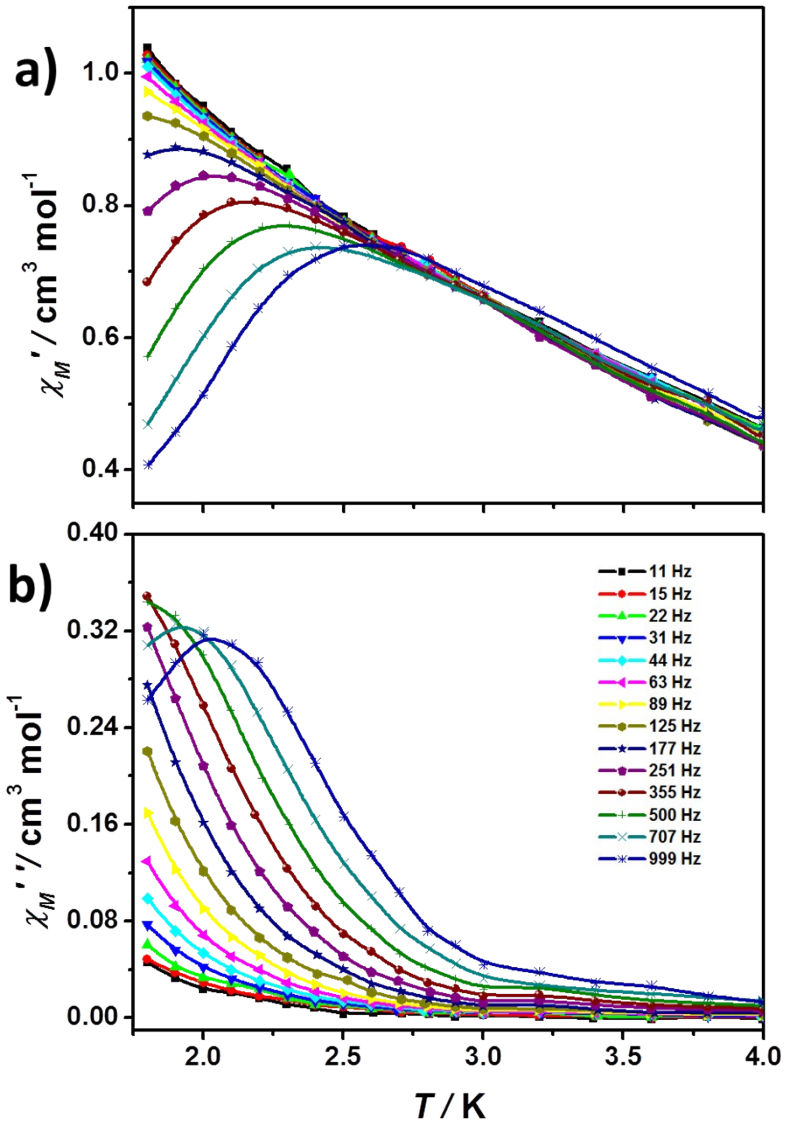

Fig. S11 Temperature dependence of in-phase (χ_M') and out-of-phase ac susceptibility (χ_M") at different ac frequencies under the dc field of 0.08 T for **1**. The solid lines are for eye guide.

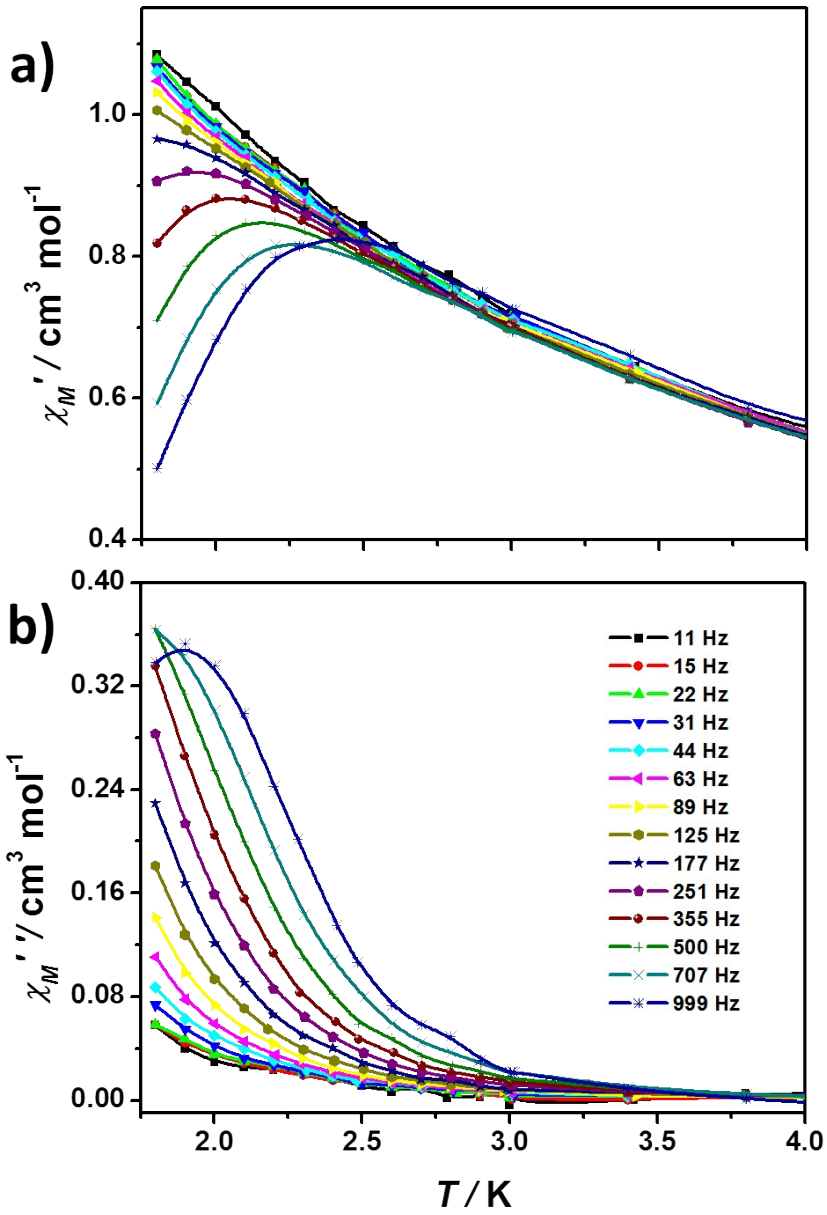

Fig. S12 Temperature dependence of in-phase (χ_M') and out-of-phase ac susceptibility (χ_M") at different ac frequencies under the dc field of 0.10 T for **2**. The solid lines are for eye guide.

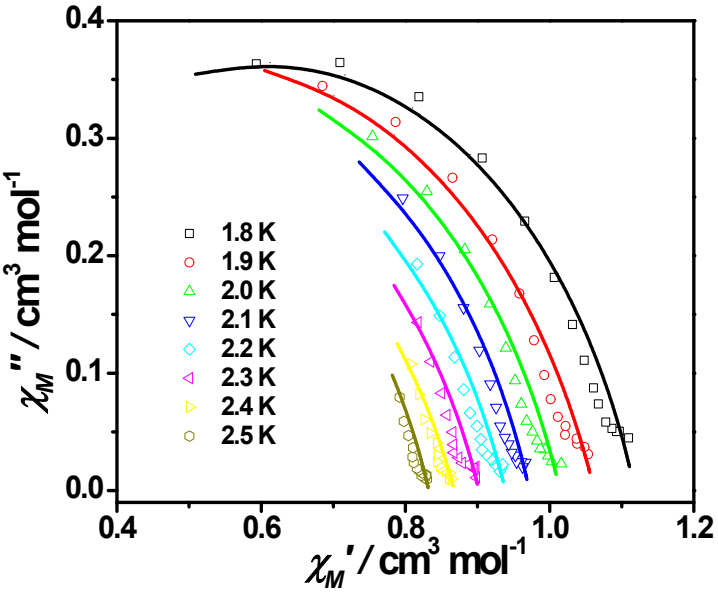

Fig. S13 Cole-Cole plot obtained from the ac susceptibility data under 0.10 T dc field in the temperature range of 1.8-2.5 K for **2**. Solid lines represent the best fits to a generalized Debye model.[S41]

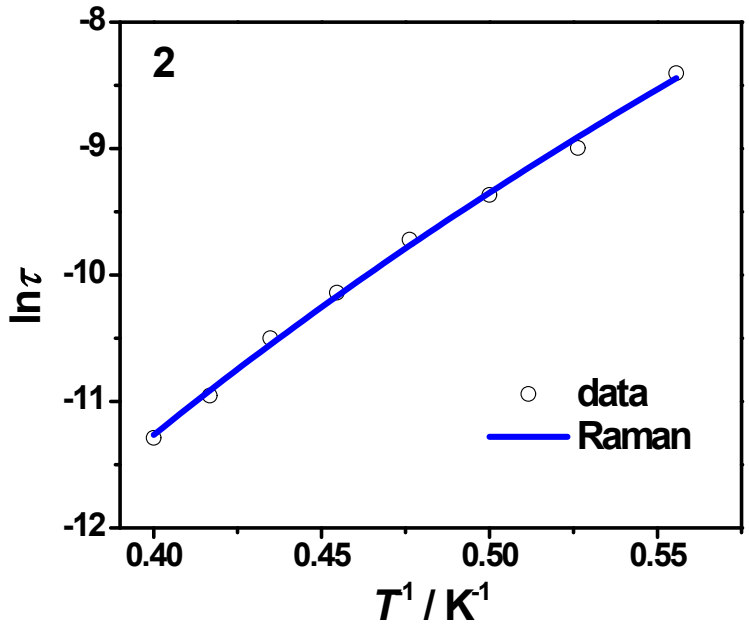

Fig. S14 Relaxation time of the magnetization *ln(τ)* vs T^{-1} plots for **2**. The solid blue line represents Raman process.

Table S6 Relaxation times τ (s) and α values for **1** and **2.**

1				
T (K)	χ_S	χ_T	τ (s)	α
1.8	0.24	1.00	0.39×10^{-3}	0.09
1.9	0.21	0.99	0.27×10^{-3}	0.11
2.0	0.17	0.95	0.19×10^{-3}	0.12
2.1	0.11	0.92	0.12×10^{-3}	0.14
2.2	0.48×10^{-3}	0.88	0.74×10^{-4}	0.16
2.3	0.16×10^{-9}	0.84	0.55×10^{-4}	0.14
2.4	0.24×10^{-9}	0.81	0.42×10^{-4}	0.13
2.5	0.38×10^{-9}	0.78	0.33×10^{-4}	0.09
2.6	0.59×10^{-9}	0.75	0.27×10^{-4}	0.05
2				
T (K)	χ_S	χ_T	τ (s)	α
1.8	0.10	1.11	0.22×10^{-3}	0.21
1.9	0.24×10^{-13}	1.06	0.12×10^{-3}	0.24
2.0	0.39×10^{-13}	1.01	0.85×10^{-4}	0.23
2.1	0.62×10^{-13}	0.97	0.60×10^{-4}	0.22
2.2	0.95×10^{-13}	0.94	0.39×10^{-4}	0.23
2.3	0.15×10^{-12}	0.90	0.27×10^{-4}	0.24
2.4	0.23×10^{-12}	0.86	0.16×10^{-4}	0.26
2.5	0.41×10^{-12}	0.83	0.12×10^{-4}	0.23

.

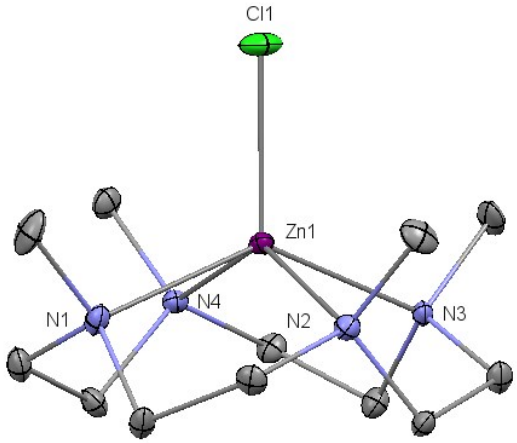

Crystal system	Monoclinic
Space group	$P\ 2_1/c$
a / Å	20.9973(15)
b / Å	10.3782(8)
c / Å	30.8762(19)
α (°)	90
β (°)	92.429(2)
γ (°)	90
V / Å^3	6722.3(8)
Z	8

Fig. S15 Structure for the anion of Zn(II) analogs of **1**. Purple, blue, green and gray spheres represent Co, N, Cl and C atoms. H atoms are omitted for clarity.

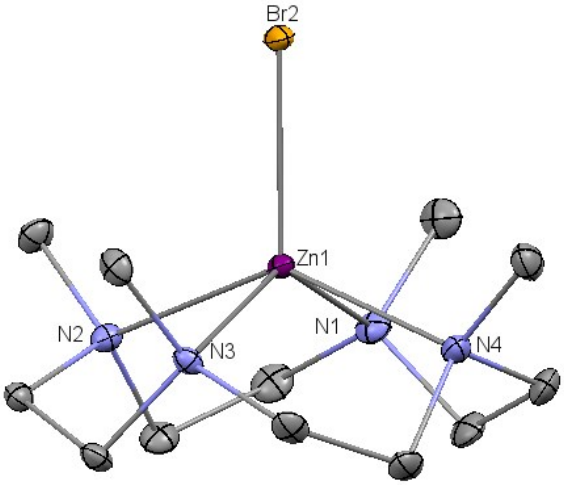

Crystal system	Monoclinic
Space group	$P\ 2_1/c$
a / Å	20.867(4)
b / Å	10.527(2)
c / Å	31.060(6)
α (°)	90.00(3)
β (°)	92.04(3)
γ (°)	90.00(3)
V / Å^3	6819(2)
Z	8

Fig. S16 Structure for the anion of Zn(II) analogs of **2**. Purple, blue, orange and gray spheres represent Co, N, Br and C atoms. H atoms are omitted for clarity.

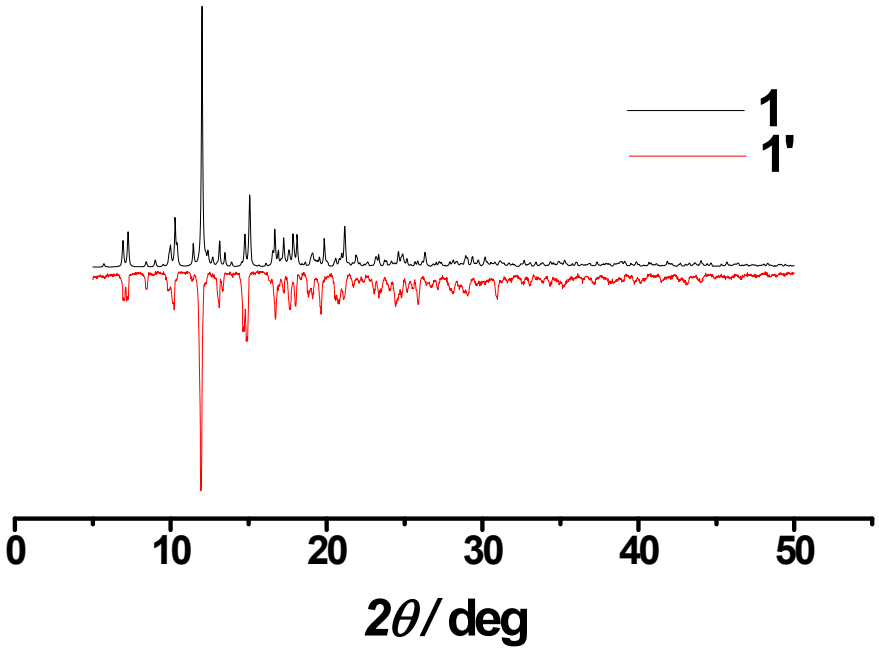

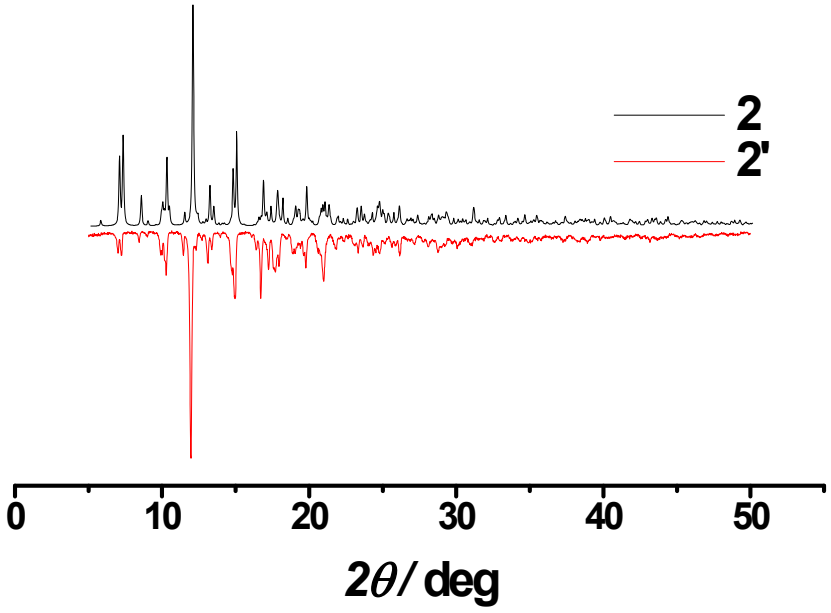

Fig. S17 XRD patterns for complexes **1'** and **2'**

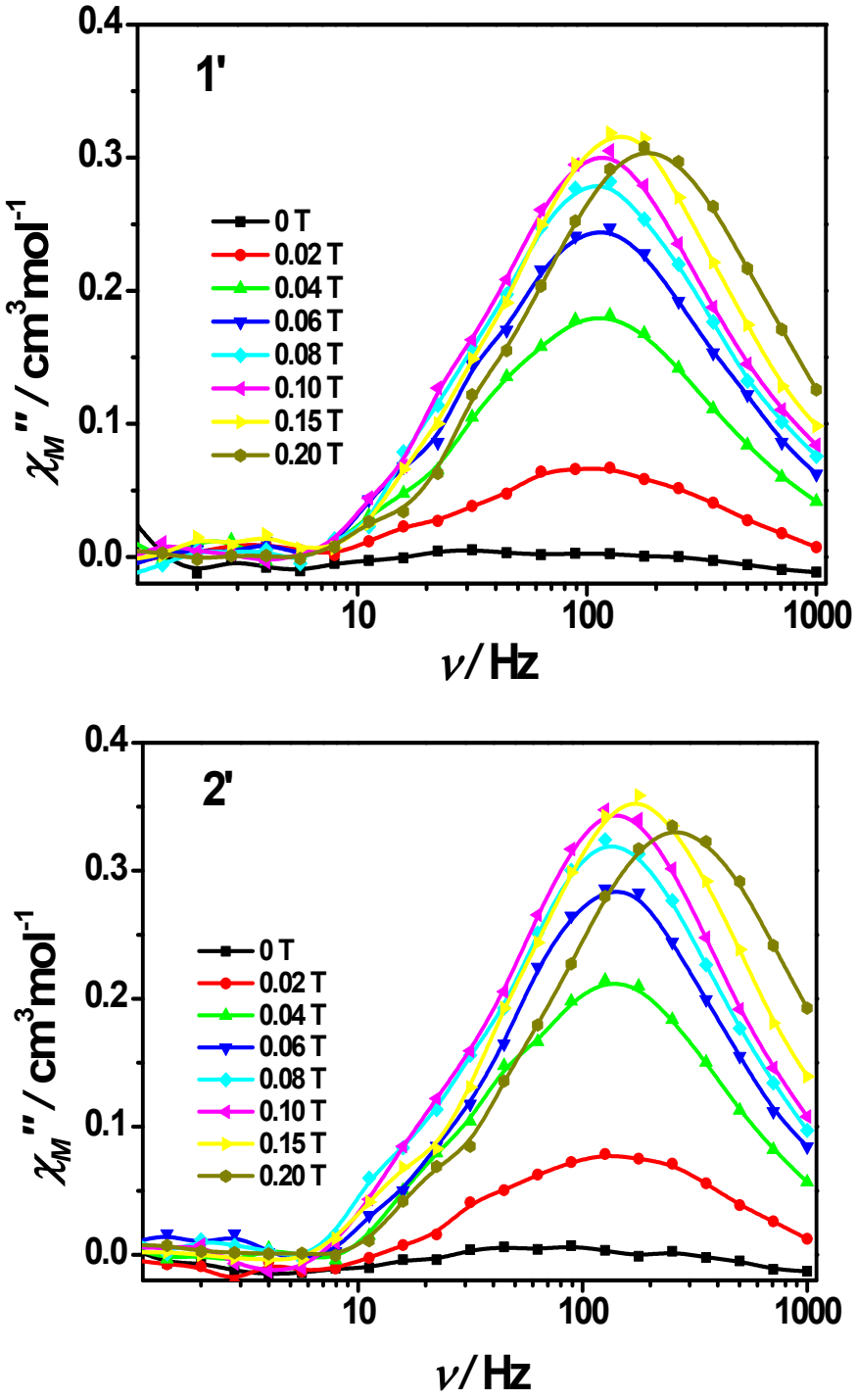

Fig. S18 Frequency dependence of out-of-phase ac susceptibility (χ_M'') at 1.8 K under the different applied static fields from 0 to 0.20 T for **1'** and **2'**. The solid lines are for eye guide.

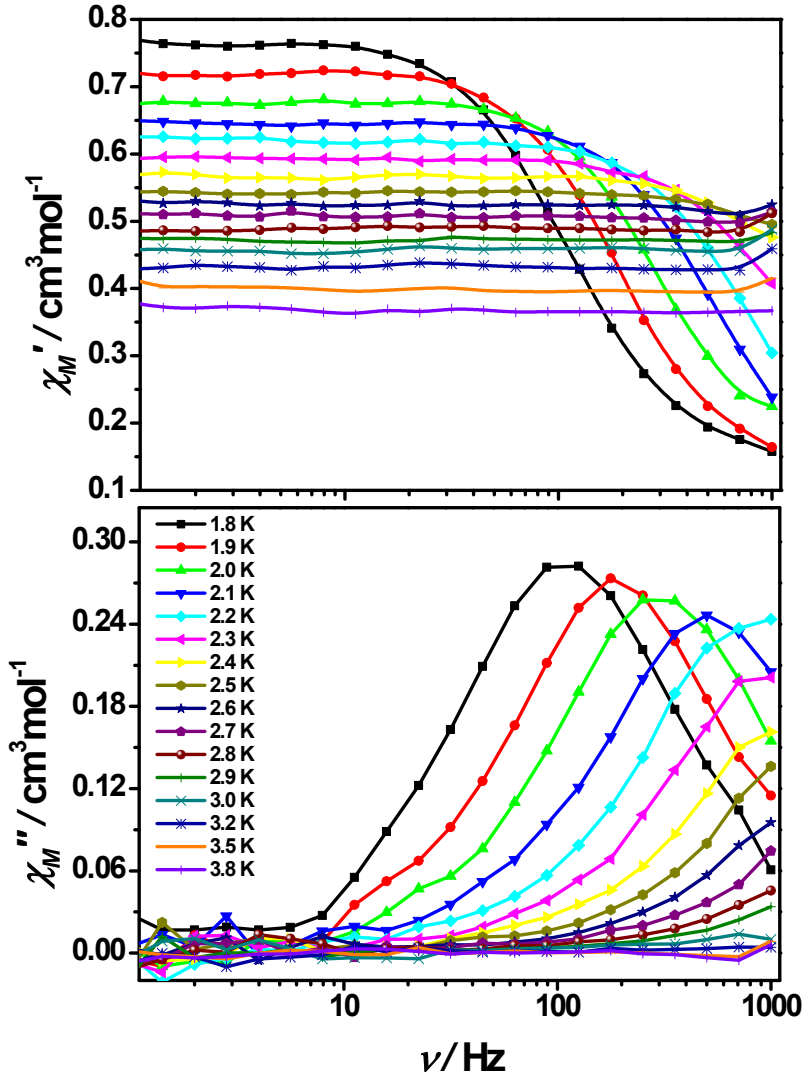

Fig. S19 Frequency dependence of the ac susceptibility from 1.8 to 3.8 K for **1'** under 0.08 T. The solid lines are for eye guide.

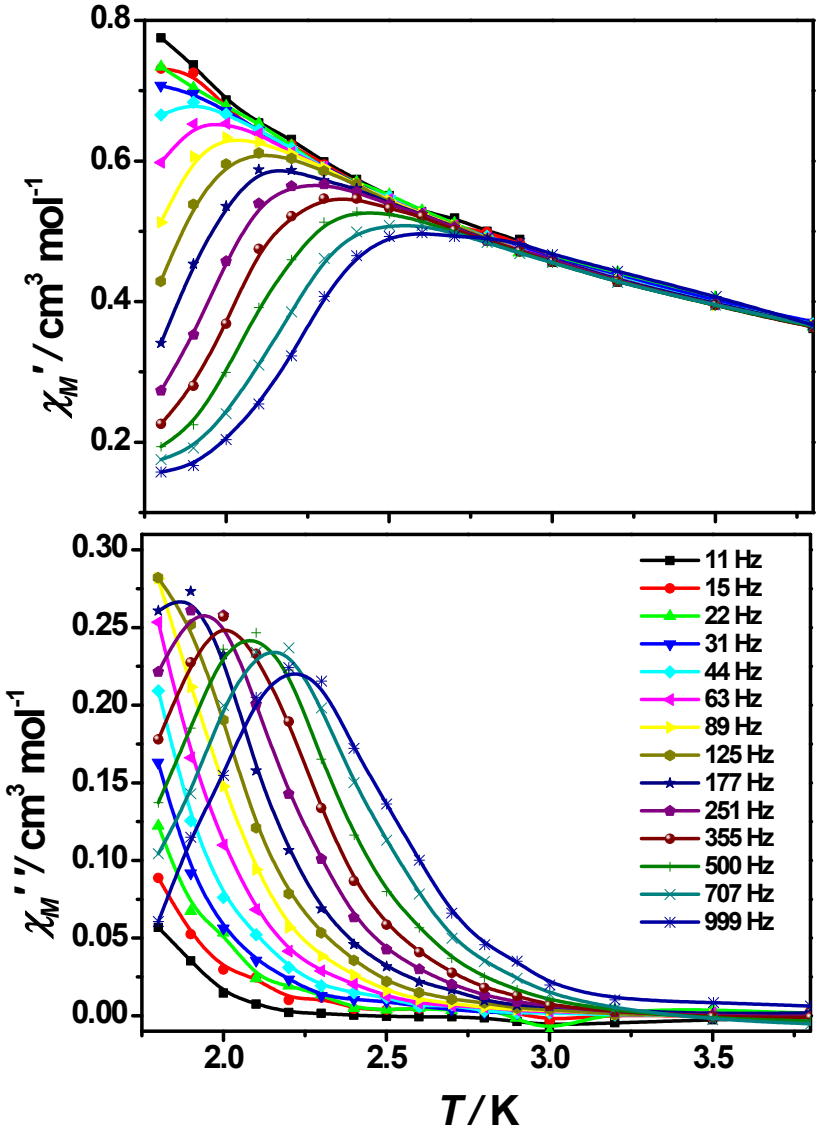

Fig. S20 Temperature dependence of ac susceptibility at different ac frequencies under 0.08 T for **1'**. The solid lines are for eye guide.

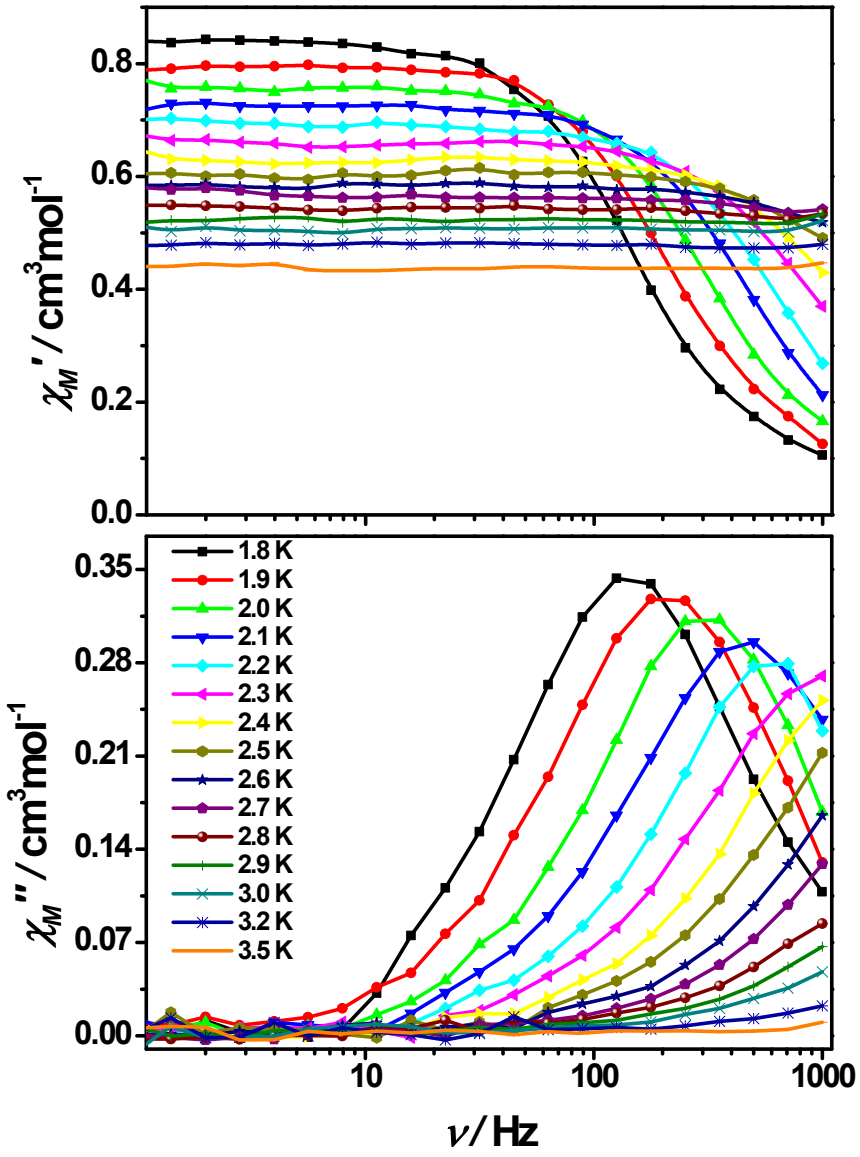

Fig. S21 Frequency dependence of the ac susceptibility from 1.8 to 3.5 K for **2'** under 0.10 T. The solid lines are for eye guide.

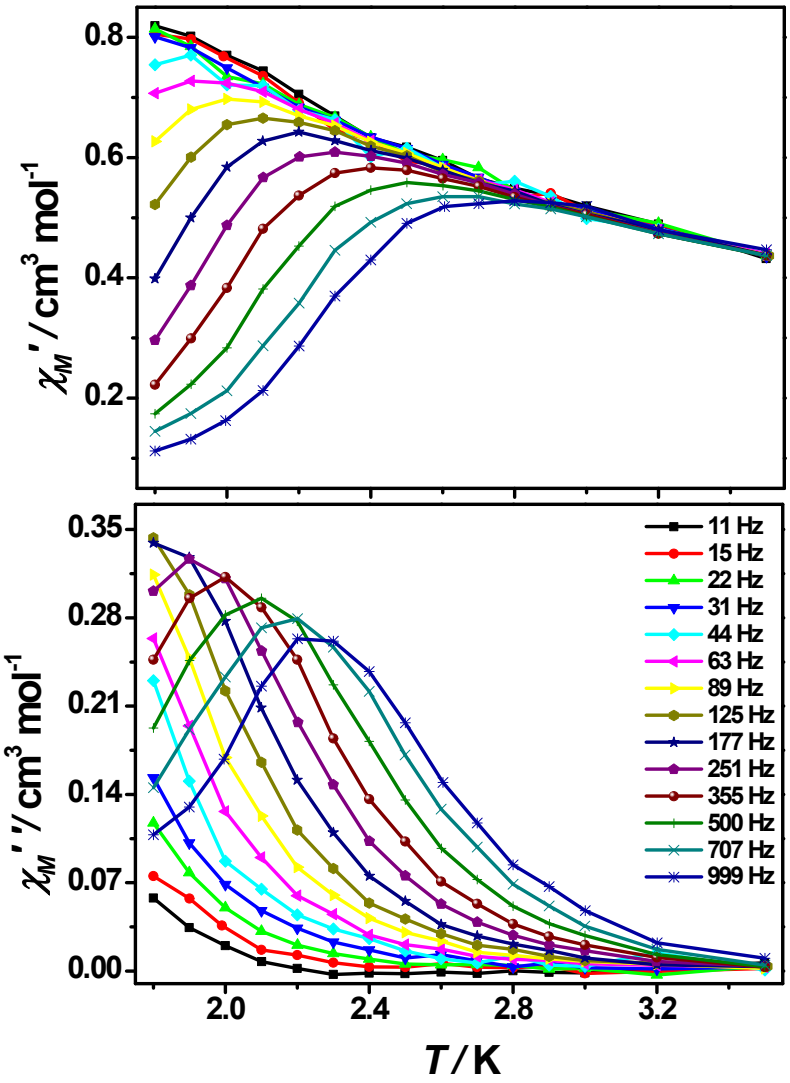

Fig. S22 Temperature dependence of ac susceptibility at different ac frequencies under 0.10 T for **2'**. The solid lines are for eye guide.

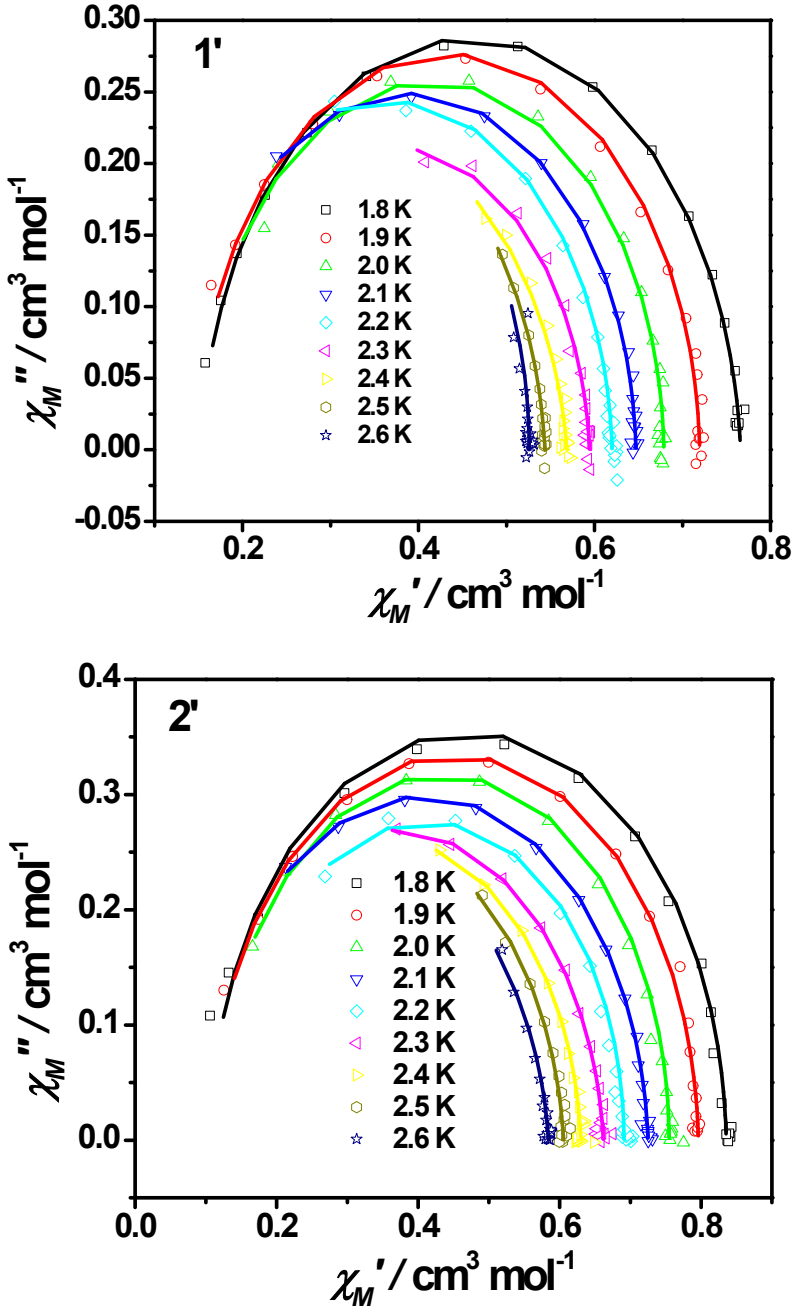

Fig. S23 Cole-Cole plot under different temperature range for **1'** and **2'**. Solid lines represent the best fits to a generalized Debye model.[S41]

Table S7 Relaxation times τ (s) and α values for **1'** and **2'.**

1'				
T (K)	χ_S	χ_T	τ (s)	α
1.8	0.15	0.77	0.13×10^{-2}	0.04
1.9	0.15	0.72	0.76×10^{-3}	0.03
2.0	0.15	0.68	0.49×10^{-3}	0.02
2.1	0.13	0.65	0.30×10^{-3}	0.03
2.2	0.10	0.62	0.20×10^{-3}	0.04
2.3	0.14	0.59	0.14×10^{-3}	0.08
2.4	0.06	0.57	0.95×10^{-4}	0.05
2.5	0.12×10^{-6}	0.54	0.73×10^{-4}	0.86×10^{-14}
2.6	0.23×10^{-6}	0.53	0.51×10^{-4}	0.89×10^{-14}
2'				
T (K)	χ_S	χ_T	τ (s)	α
1.8	0.11	0.83	0.11×10^{-2}	0.02
1.9	0.11	0.80	0.76×10^{-3}	0.02
2.0	0.11	0.75	0.53×10^{-3}	0.005
2.1	0.09	0.72	0.35×10^{-3}	0.04
2.2	0.13	0.69	0.28×10^{-3}	0.002
2.3	0.07	0.66	0.16×10^{-3}	0.06
2.4	0.07	0.63	0.11×10^{-3}	0.04
2.5	0.02	0.60	0.74×10^{-4}	0.05
2.6	0.30×10^{-5}	0.58	0.49×10^{-4}	0.07

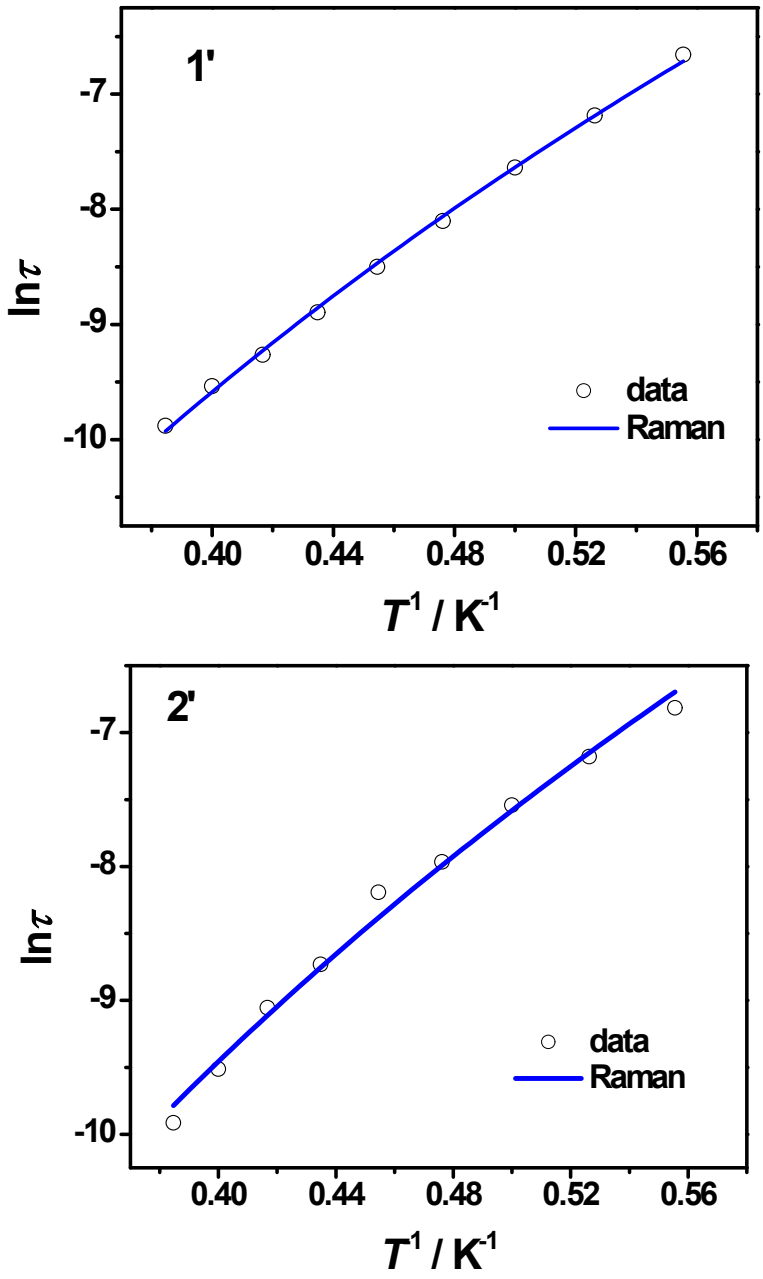

Fig. S24 The plot of *ln(τ)* versus T^{-1} for **1'** and **2'**.

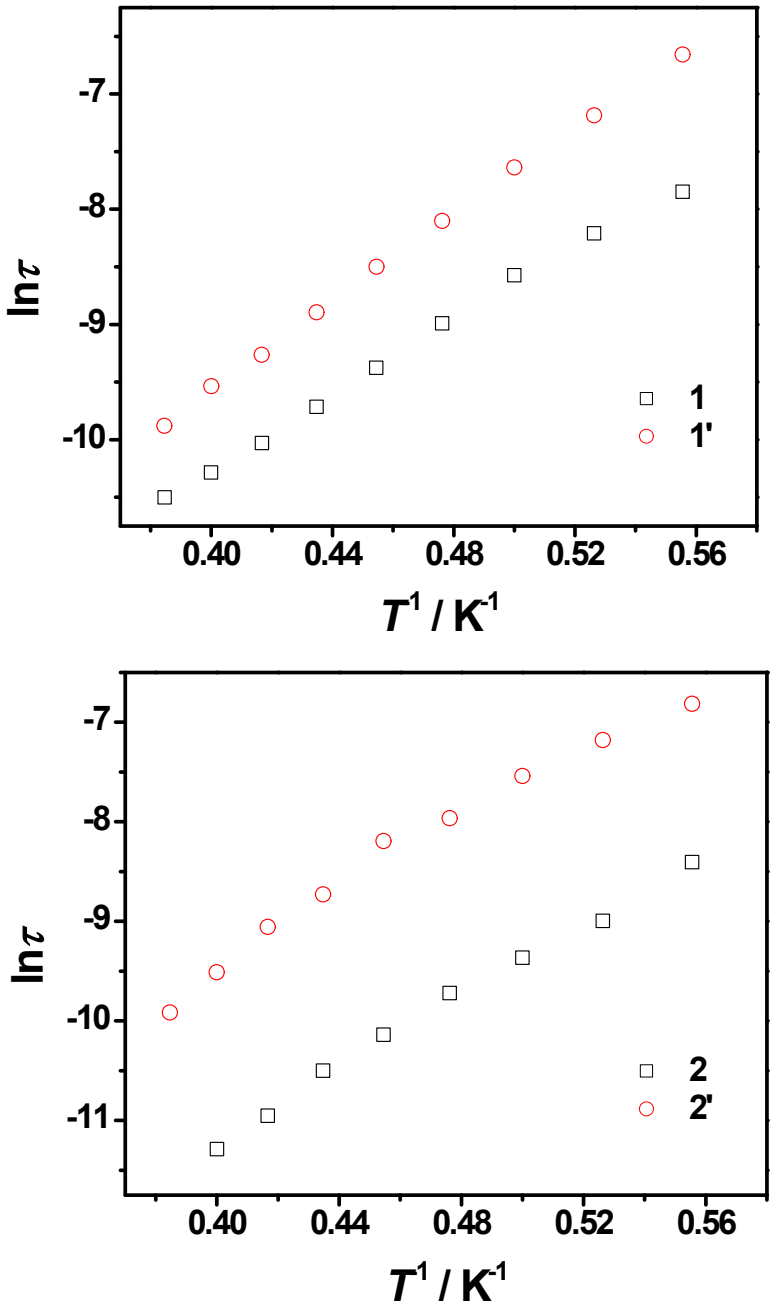

Fig. S25 Relaxation times in **1**, **1'**, **2** and **2'**.

Computational details

Mononuclear complex **3** has one type of molecular structure, but complexes **1** and **2** both have two types indicated as **1*a***, **1*b***, **2*a*** and **2*b***, respectively. Complete active space second-order multiconfigurational perturbation theory (CASPT2) considering the effect of the dynamic electron correlation based on complete-active-space self-consistent field (CASSCF) method with MOLCAS 8.4 program package[S42] was performed on the basis of single-crystal X-ray determined geometries of complexes **1**−**3**, which are oriented with respect to a reference frame shown in Figure S26.

For the first CASSCF calculation, the basis sets for all atoms are atomic natural orbitals from the MOLCAS ANO-RCC library: ANO-RCC-VTZP for magnetic center ion Co^{II}; VTZ for close N atoms; VDZ for distant atoms. The calculations employed the second order Douglas-Kroll-Hess Hamiltonian, where scalar relativistic contractions were taken into account in the basis set. The effect of the dynamical electronic correlation was applied using CASPT2 based on the first CASSCF calculation. After that, the spin-orbit coupling was handled separately in the restricted active space state interaction (RASSI-SO) procedure. For all complexes, the active electrons in 5+5′ active spaces include all *d* electrons (CAS(7 in 5+5′)) in the CASSCF calculations. To exclude all the doubts, we calculated all the roots in the active space. We have mixed the maximum number of spin-free state which was possible with our hardware (all from 10 quadruplets and 20 from 40 doublets). SINGLE_ANISO[S43] program was used to obtain zero-field splitting parameters *D* (*E*) (cm^{-1}), ***g*** tensors, energy levels, magnetic axes, *et al.,* based on the above

CASPT2/RASSI-SO calculations.

To deeply analyze the magnetic anisotropies of complexes **1**–**3**, ORCA 4.2 calculations[S44] were performed with complete active space self-consistent field calculations (CASSCF), followed by N-electron valence second-order perturbation theory (NEVPT2). The spin-orbit coupling (SOC) operator used was the efficient implementation of the multicenter spin-orbit mean-field (SOMF) concept developed by Hess et al.[S45] The spin-spin contributions (SSC) to the *D* values were also included although they are very small for our complexes. The NEVPT2[S46-S49] calculation both with seven 3d electrons in five Co 3d-based orbitals (CAS(7, 5+5′)) including 3d-double shell effects were performed on complexes **1**–**3**. In the calculations, the orbitals were determined for the average of 10 $S = 3/2$ and 40 $S = 1/2$ roots. All calculations were performed with triple-ζ with one polarization function def2-TZVP basis set for all atoms. [S50-S52]

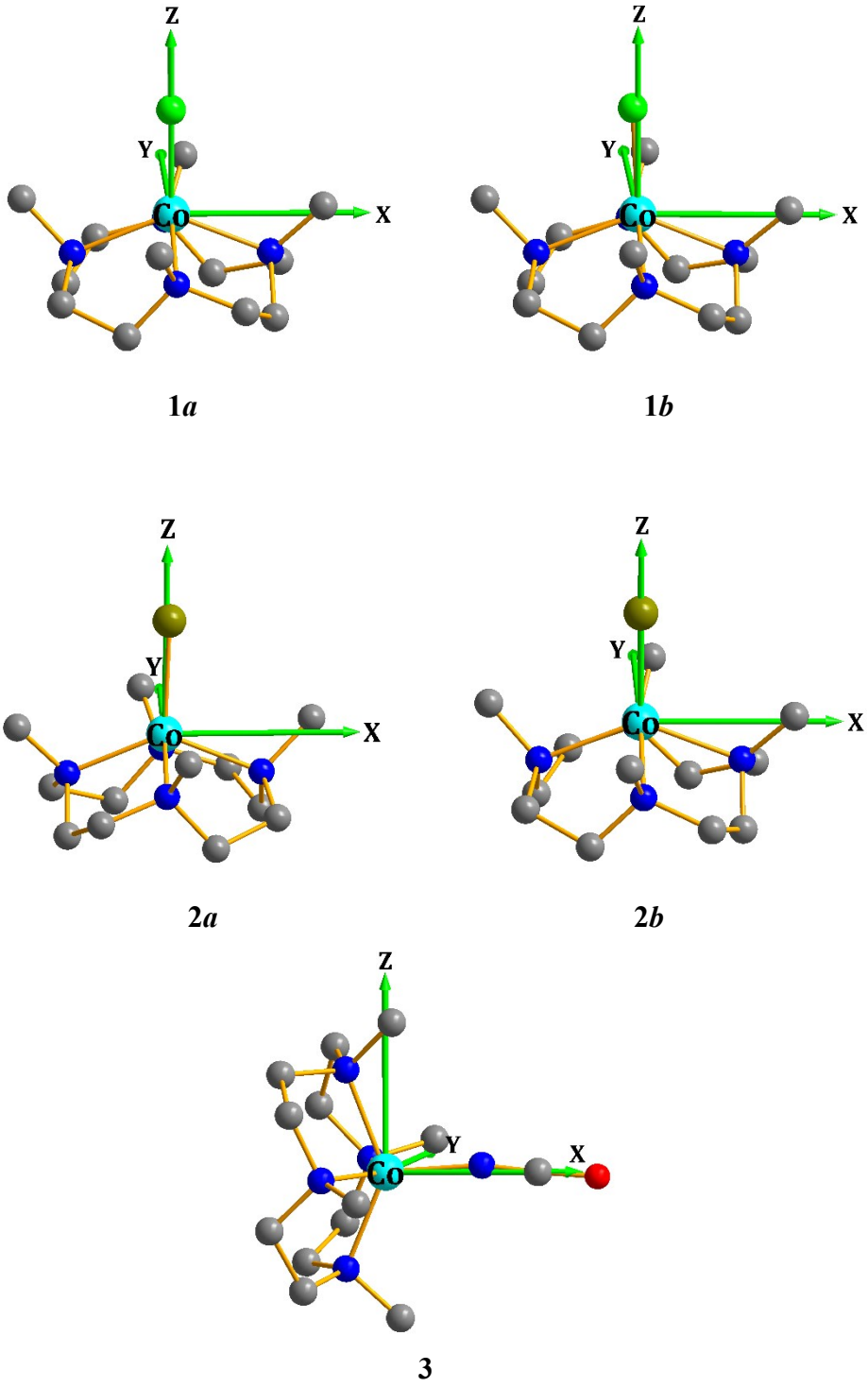

Fig. S26 Calculated complete structures of **1**–**3**. H atoms are omitted for clarity.

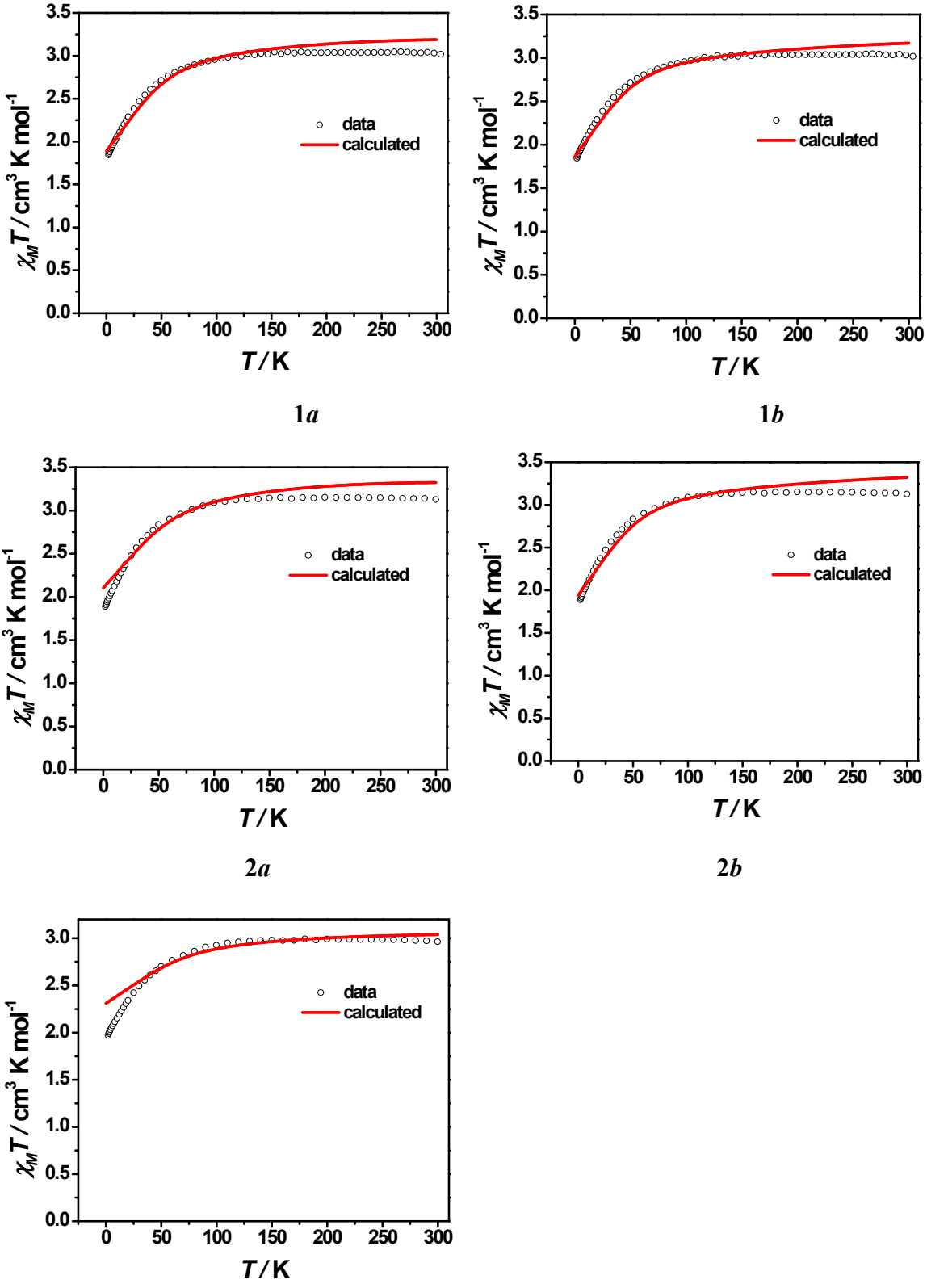

Fig. S27 Calculated (red solid line) data of magnetic susceptibilities of complexes **1**–**3**.

Table S8 Calculated spin-free energies (cm^{-1}) of the lowest ten terms (S = 3/2) of the Co^{II} ion of complexes **1-3** using CASPT2/RASSI-SO with MOLCAS 8.4.

spin-free states	**1*a***	**1*b***	**2*a***	**2*b***	**3**
	E/cm^{-1}	E/cm^{-1}	E/cm^{-1}	E/cm^{-1}	E/cm^{-1}
1	0.0	0.0	0.0	0.0	0.0
2	427.9	611.5	283.8	667.5	375.7
3	480.0	763.5	511.9	765.2	1306.5
4	3444.6	3409.4	3144.4	3286.0	3095.4
5	7302.7	7477.8	7117.6	7325.3	7620.8
6	8051.4	7791.3	7682.7	7603.7	7973.2
7	10237.3	10049.7	10027.4	9934.3	10720.3
8	17485.1	17339.2	17434.3	17243.6	17326.4
9	17638.4	17502.9	17484.3	17527.0	17906.7
10	19362.5	19185.3	19926.7	19728.3	19138.7

Table S9 Calculated weights of the five most important spin-orbit states for the lowest two spin-orbit states of complexes **1-3** using CASPT2/RASSI-SO with MOLCAS 8.4.

	Spin-orbit states	Energy (cm^{-1})	Spin-free states, Spin, Weights				
1*a*	1	0.0	1,1.5,0.6920	3,1.5,0.1710	2,1.5,0.1324	4,1.5,0.0022	14,0.5,0.0007
	2	118.1	1,1.5,0.7012	2,1.5,0.1680	3,1.5,0.1229	4,1.5,0.0046	7,1.5,0.0013
1*b*	1	0.0	1,1.5,0.7505	2,1.5,0.1503	3,1.5,0.0944	4,1.5,0.0025	15,0.5,0.0006
	2	114.0	1,1.5,0.7990	3,1.5,0.0989	2,1.5,0.0948	4,1.5,0.0035	7,1.5,0.0015
2*a*	1	0.0	1,1.5,0.6538	2,1.5,0.2661	3,1.5,0.0761	4,1.5,0.0029	5,1.5,0.0005
	2	135.0	1,1.5,0.6859	3,1.5,0.1792	2,1.5,0.1283	4,1.5,0.0051	7,1.5,0.0013
2*b*	1	0.0	1,1.5,0.7672	2,1.5,0.1373	3,1.5,0.0924	4,1.5,0.0021	5,1.5,0.0003
	2	118.0	1,1.5,0.8117	3,1.5,0.0945	2,1.5,0.0882	4,1.5,0.0033	7,1.5,0.0016
3	1	0.0	1,1.5,0.6853	2,1.5,0.2837	3,1.5,0.0218	4,1.5,0.0066	5,1.5,0.0005
	2	162.3	1,1.5,0.8444	2,1.5,0.0827	3,1.5,0.0649	4,1.5,0.0038	5,1.5,0.0011

Table S10 Contribution of the excited states (with relative energy, cm^{-1}) to *D* values (cm^{-1}) for complexes **1-3** using NEVPT2 with ORCA 4.2.

complexes	State No.	Mult	Energy, cm^{-1}	Contribution, cm^{-1}
				D
1*a*	1	4	404.6	55.2
	2	4	566.3	43.4
	4	4	6063.0	–3.0
	6	4	8116.5	–8.5
	1	2	17351.3	–1.4
	2	2	17783.6	–1.1
	4	2	19928.3	–1.1
1*b*	1	4	461.4	50.3
	2	4	617.5	48.3
	5	4	6445.3	–2.2
	6	4	8051.0	–8.4
	1	2	17556.6	–1.4
	2	2	17781.5	–1.2
	4	2	19882.9	–1.3
2*a*	1	4	481.8	52.1
	2	4	690.3	43.8
	6	4	8003.0	–10.3
	1	2	17267.4	–1.6
	2	2	17598.3	–1.4
	6	2	20277.4	–1.5
	7	2	20448.3	–2.1
2*b*	1	4	607.4	46.1
	2	4	676.8	45.4

	5	4	6425.3	–1.8
	6	4	7936.3	–9.6
	1	2	17444.3	–1.5
	6	2	20355.2	–1.8
	7	2	20419.9	–1.7
3	1	4	263.2	–86.2
	3	4	2597.9	–10.7
	4	4	6150.7	3.7
	6	4	8690.0	0.6
	1	2	17952.3	0.6
	6	2	19981.2	0.7
	7	2	20647.8	0.8

Table S11 Relative energies (cm^{-1}) of ligand field one-electron states (in the basis of d-AOs) of complexes **1-3** from AILFT analysis using NEVPT2 with ORCA 4.2.

complexes	No.	LF one-electron state	Energy, cm^{-1}
1*a*	1	1.00 d_{xy}	0.0
	2	0.91 d_{yz} + 0.40 d_{z2}	1973.6
	3	0.96 d_{xz} + 0.27 d_{z2}	2352.8
	4	0.87 d_{z2} – 0.40 d_{yz} – 0.28 d_{xz}	2666.4
	5	1.00 d_{x2-y2}	8025.2
1*b*	1	–1.00 d_{xy}	0.0
	2	0.72 d_{xz} – 0.54 d_{z2} + 0.43 d_{yz}	2075.3
	3	0.86 d_{yz} – 0.50 d_{xz}	2319.0
	4	– 0.84 d_{z2} – 0.48 d_{xz} – 0.26 d_{yz}	2826.3
	5	1.00 d_{x2-y2}	7946.1
2*a*	1	1.00 d_{xy}	0.0
	2	0.80 d_{yz} + 0.57 d_{z2} + 0.17 d_{xz}	1604.0
	3	– 0.62 d_{z2} + 0.57 d_{yz} – 0.54 d_{xz}	1813.4
	4	–0.82 d_{xz} + 0.53 d_{z2} – 0.20 d_{yz}	2091.7
	5	1.00 d_{x2-y2}	7969.1
2*b*	1	0.99 d_{xy}	0.0
	2	0.71 d_{yz} + 0.68 d_{z2} – 0.16 d_{xz}	1659.0
	3	–0.98 d_{xz} – 0.13 d_{z2}	1996.3
	4	–0.72 d_{z2} + 0.70 d_{yz}	2246.7
	5	1.00 d_{x2-y2}	7892.1
3	1	1.00 d_{yz}	0.0
	2	0.92 d_{xy} + 0.25 d_{xz} + 0.26 d_{x2-y2}	2157.8
	3	–0.92 d_{xz} + 0.32 d_{xy} – 0.22 d_{x2-y2}	2546.8
	4	0.80 d_{x2-y2} – 0.47 d_{z2} – 0.28 d_{xz} – 0.22 d_{xy}	4054.0
	5	0.87 d_{z2} + 0.48 d_{x2-y2}	7935.7

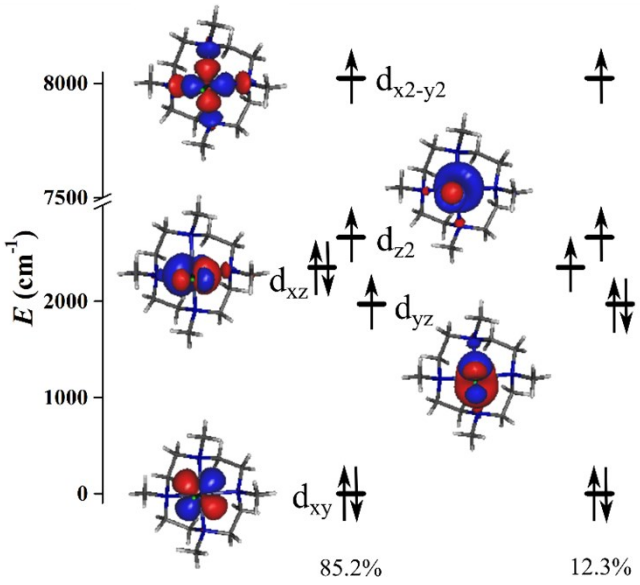
8000
7500
2000
1000
0
E (cm-1)
dx2-y2
dz2
dxz
dyz
dxy
85.2%
12.3%

1*a*

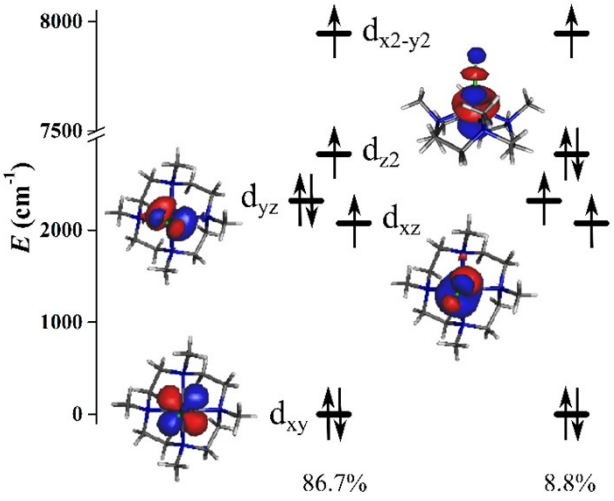
8000
7500
2000
1000
0
E (cm-1)
dx2-y2
dz2
dyz
dxz
dxy
86.7%
8.8%

1*b*

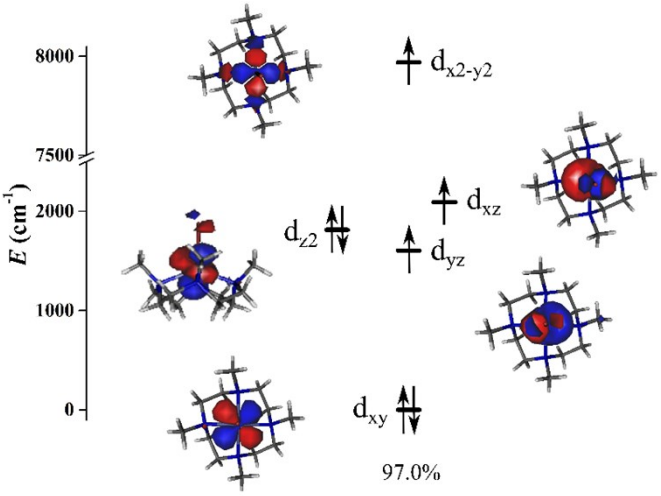
8000
7500
2000
1000
0
E (cm-1)
dx2-y2
dz2
dxz
dyz
dxy
97.0%

2*a*

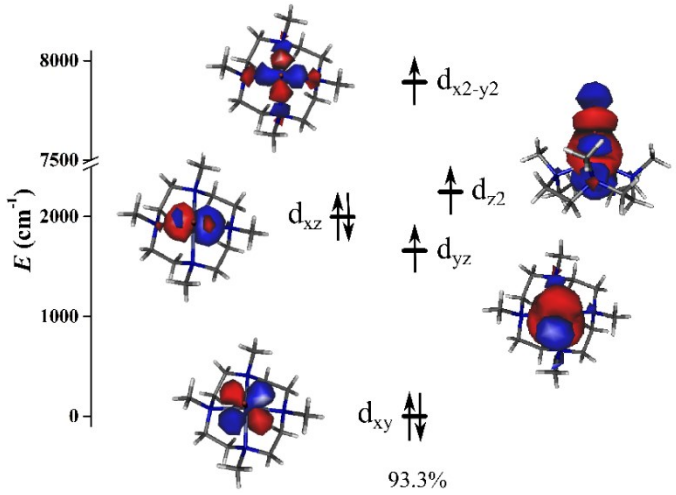

2b

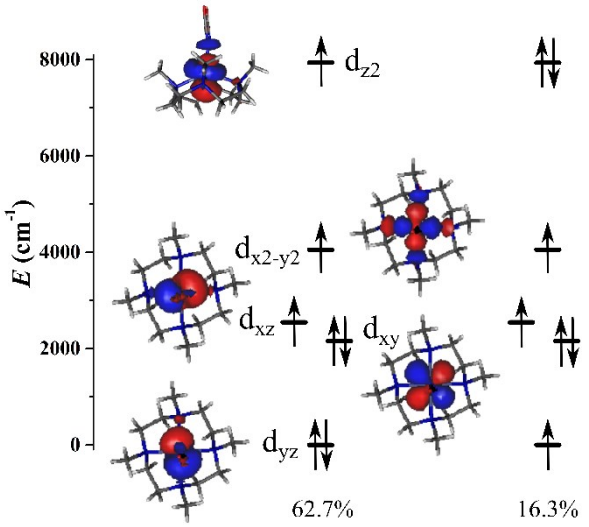

3

Fig. S28 Orbital energies computed for the ground state of complex **1-3** using NEVPT2 with ORCA 4.2.[S53-S54] The percentage mention reveals the percent of the corresponding configuration mixing.

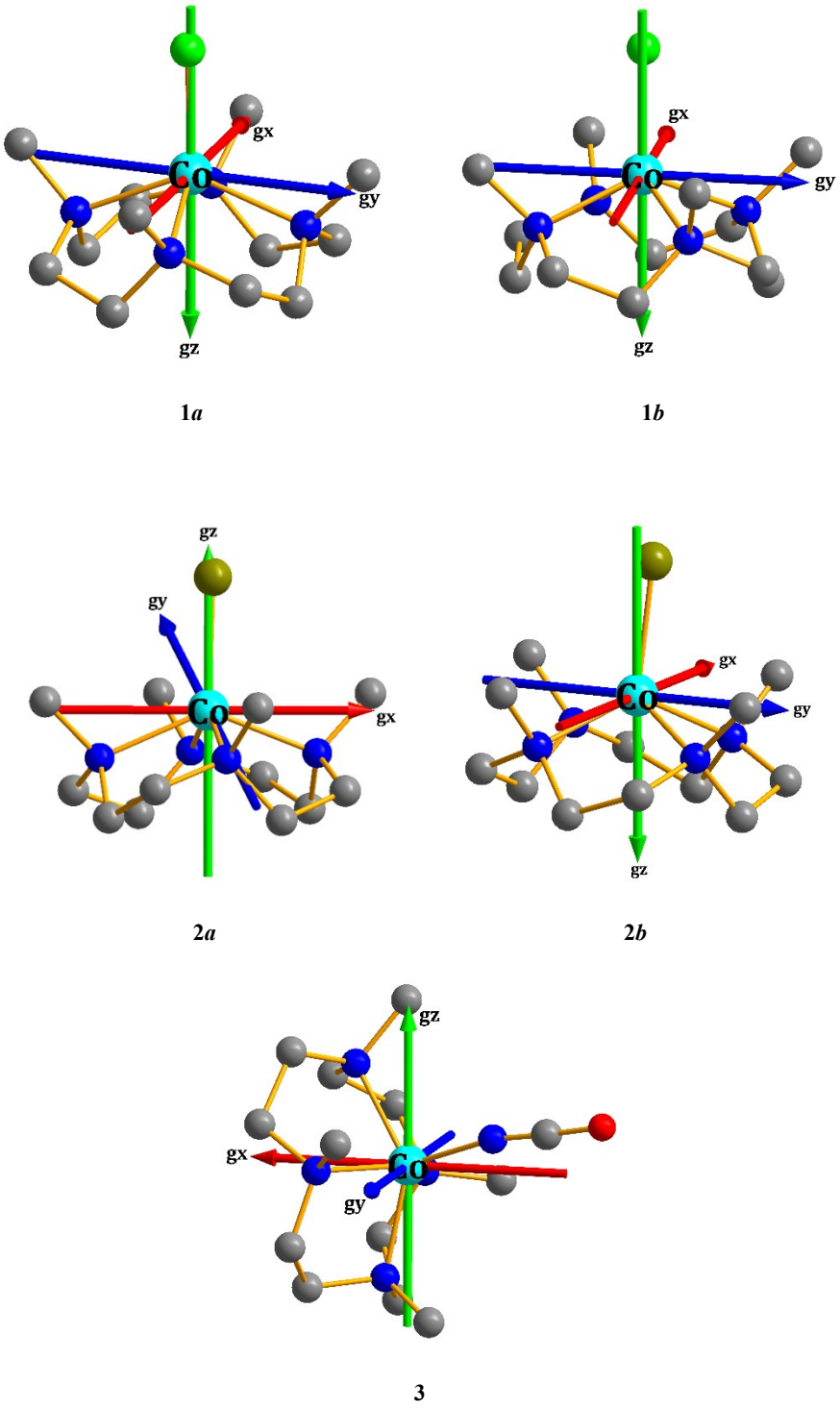

Fig. S29. Orientations of the local magnetic axes (red: g_x; blue: g_y; green: g_z) on Co^{II} ions of **1**–**3** in their ground spin-orbit states.

References

S1 F. Habib, O. R. Luca, V. Vieru, M. Shiddiq, I. Korobkov, S. I. Gorelsky, M. K. Takase, L. F. Chibotaru, S. Hill, R. H. Crabtree and M. Murugesu, *Angew. Chem. Int. Ed.*, 2013, **52**, 11290–11293.

S2 R. F. Higgins, B. N. Livesay, T. J. Ozumerzifon, J. P. Joyce, A. K. Rappé and M. P. Shores, *Polyhedron*, 2018, **143**, 193–200.

S3 T. Jurca, A. Farghal, P.-H. Lin, I. Korobkov, M. Murugesu, and D. S. Richeson, *J. Am. Chem. Soc.*, 2011, **133**, 15814–15817.

S4 J.-J. Liu, Y.-S. Meng, I. Hlavička, M. Orlita, S.-D Jiang, B.-W. Wang and S. Gao, *Dalton Trans.*, 2017, **46**, 7408–7411.

S5 I. Nemec, H. Liu, R. Herchel, X. Zhang and Z. Trávníček, *Syn. Metal.*, 2016, **215**, 158–163.

S6 A. K. Mondal, T. Goswami, A. Misra and S. Konar, *Inorg. Chem.*, 2017, **56**, 6870−6878.

S7 C. Rajnák, F. Varga, J. Titiš, J. Moncoľ and R. Boča, *Eur. J. Inorg. Chem.*, 2017, 1915–1922.

S8 B. Brachňaková, S. Matejová, J. Moncol, R. Herchel, J. Pavlik, E. Moreno-Pineda, M. Ruben and I. Šalitroš, *Dalton Trans.*, 2020, **49**, 1249–1264.

S9 A. Świtlicka, B. Machura, M. Penkala, A. Bieńko, D. C. Bieńko, J. Titiš, C. Rajnák, R. Boča, A. Ozarowski and M. Ozerov, *Inorg. Chem.*, 2018, **57**, 12740−12755.

S10 C. Rajnák, J. Titiš, O. Fuhr, M. Ruben and R. Boča, *Inorg. Chem.*, 2014, **53**,

8200−8202.

S11 C. Rajnák, J. Titiš, J. Miklovič, G. E. Kostakis, O. Fuhr, M. Ruben and R. Boča, *Polyhedron*, 2017, **126**, 174–183.

S12 Y. Cui, Y. Xu, X. Liu, Y. Li, B.-L. Wang, Y. Dong, W. Li and S. Lei, *Chem. Asian J.*, 2019, **14**, 2620–2628.

S13 Y. Cui, Y. Ge, Y. Li, J. Yao and Y. Dong, *Struct. Chem.*, 2020. DOI: 10.1007/s11224-019-01429-3

S14 I. Nemec, R. Herchel and Z. Trávníček, *Dalton Trans.*, 2016, **45**, 12479–12482.

S15 J. Acharya, A. Sarkar, P. Kumar, V.Kumar, J. F. Gonzalez, O. Cador, F. Pointillart, G. Rajaraman and V. Chandrasekhar, *Dalton Trans.*, 2020, **49**, 4785–4796.

S16 I. Banerjee, A. Jana, S. Singh, J. Marek, E. del Barco, M. Ali, *Polyhedron*, 2013, **66**, 162−166.

S17 D. M. Piñero Cruz, D. N. Woodruff, I.-R. Jeon, I. Bhowmick, M. Secu, E. A. Hillard, P. Dechambenoit and R. Clérac, *New J. Chem.*, 2014, **38**, 3443−3448.

S18 A. Packová, J. Miklovič and R. Boča, *Polyhedron*, 2015, **102**, 88–93.

S19 R. Ruamps, L. J. Batchelor, R. Guillot, G. Zakhia, A.-L. Barra, W. Wernsdorfer, N. Guihéry and T. Mallah, *Chem. Sci.*, 2014, **5**, 3418–3424.

S20 K. A. Schulte, K. R. Vignesh and K. R. Dunbar, *Chem. Sci.*, 2018, **9**, 9018–9026.

S21 F. Shao, B. Cahier, N. Guihéry, E. Rivière, R. Guillot, A.-L. Barra, Y. Lan, W.

Wernsdorfer, V. E. Campbell and T. Mallah, *Chem. Commun.*, 2015, **51**, 16475–16478.

S22 F. Shao, B. Cahier, Y.-T. Wang, F.-L. Yang, E. RiviHre, R. Guillot, N. Guihéry, J.-P. Tong, and T. Mallah, *Chem. Asian J.*, 2020, **15**, 391–397.

S23 F. Shao, B. Cahier, E. Rivière, R. Guillot, N. Guihéry, V. E. Campbell and T. Mallah, *Inorg. Chem.*, 2017, **56**, 1104−1111.

S24 D. Schweinfurth, M. G. Sommer, M. Atanasov, S. Demeshko, S. Hohloch, F. Meyer, F. Neese and B. Sarkar, *J. Am. Chem. Soc.*, 2015, **137**, 1993−2005.

S25 A. K. Mondal, J. Jover, E. Ruiz and S. Konar, *Chem. Eur. J.*, 2017, **23**, 12550–12558.

S26 T. J. Woods, M. F. Ballesteros-Rivas, S. Gómez-Coca, E. Ruiz and K. R. Dunbar, *J. Am. Chem. Soc.*, 2016, **138**, 16407−16416.

S27 F. El-Khatib, B. Cahier, F. Shao, M. López-Jordà, R. Guillot, E. Rivière, H. Hafez, Z. Saad, J.-J. Girerd, N. Guihéry and T. Mallah, *Inorg. Chem.*, 2017, **56**, 4601−4608.

S28 A. Collet, G. A. Craig, M. J. H. Ojea, L. Bhaskaran, C. Wilson, S. Hill and M. Murrie, *Dalton Trans.*, 2018, **47**, 9237–9240.

S29 M. A. Hay, A. Sarkar, G. A. Craig, L. Bhaskaran, J. Nehrkorn, M. Ozerov, K. E. R. Marriott, C. Wilson, G. Rajaraman, S. Hill and M. Murrie, *Chem. Sci.*, 2019, **10**, 6354–6361.

S30 N. Nedelko, A. Kornowicz, I. Justyniak, P. Aleshkevych, D. Prochowicz, P. Krupiński, O. Dorosh, A. Ślawska-Waniewska, and J. Lewiński, *Inorg. Chem.*,

2014, **53**, 12870−12876.

S31 I. Nemec, R. Marx, R. Herchel, P. Neugebauer, J. van Slagerenb and Z. Trávníček, *Dalton Trans.*, 2015, **44**, 15014–15021.

S32 X. Hou, X. Wang, X. Liu, J. Wang, L. Tang and P. Ju, *New J. Chem.*, 2018, **42**, 8583–8590.

S33 A. K. Mondal, J. Jover, E. Ruiz and S. Konar, *Chem. Commun.*, 2017, **53**, 5338–5341.

S34 A. K. Mondal, J. Jover, E. Ruiz and S. Konar, *Dalton Trans.*, 2019, **48**, 25–29.

S35 S. Mandal, S. Mondal, C. Rajnák, J. Titiš, R. Boča and S. Mohanta, *Dalton Trans.*, 2017, **46**, 13135–13144.

S36 A. K. Mondal, A. Mondal and S. Konar, *Magnetochemistry*, 2019, **5**, 12(1-11).

S37 H.-H. Cui, J. Wang, X.-T. Chen and Z.-L. Xue, *Chem. Commun.*, 2017, **53**, 9304–9307.

S38 H.-H. Cui, Y.-Q. Zhang, X.-T. Chen, Z. Wang and Z.-L. Xue, *Dalton Trans.*, 2019, **48**, 10743–10752.

S39 (a) M. Llunell, D. Casanova, J. Cirera, P. Alemany and S. Alvarez, *Shape Program*, Version 2.1, 2013; (b) S. Alvarez, P. Alemany, D. Casanova, J. Cirera, M. Llunell and D. Avnir, *Coord. Chem. Rev.*, 2005, **249**, 1693-1708.

S40 N. F. Chilton, R. P. Anderson, L. D. Turner, A. Soncini and K. S. Murray, *J. Comput. Chem.*, 2013, **34**, 1164−1175.

S41 (a) K. S. Cole and R. H. Cole, *J. Chem. Phys.*, 1941, **9**, 341−351; (b) Y.-N. Guo, G.-F. Xu, Y. Guo and J. Tang, *Dalton Trans.*, 2011, **40**, 9953–9963.

S42 F. Aquilante, J. Autschbach, R. K. Carlson, L. F. Chibotaru, M. G. Delcey, L. De Vico, I. Fdez. Galván, N. Ferré, L. M. Frutos, L. Gagliardi, M. Garavelli, A. Giussani, C. E. Hoyer, G. Li Manni, H. Lischka, D. Ma, P. Å. Malmqvist, T. Müller, A. Nenov, M. Olivucci, T. B. Pedersen, D. Peng, F. Plasser, B. Pritchard, M. Reiher, I. Rivalta, I. Schapiro, J. Segarra-Martí, M. Stenrup, D. G. Truhlar, L. Ungur, A. Valentini, S. Vancoillie, V. Veryazov, V. P. Vysotskiy, O. Weingart, F. Zapata and R. Lindh, *J. Comput. Chem.*, 2016, **37**, 506–541.

S43 (a) L. F. Chibotaru, L. Ungur and A. Soncini, *Angew. Chem. Int. Ed.*, 2008, **47**, 4126–4129. (b) L. Ungur, W. Van den Heuvel and L. F. Chibotaru, *New J. Chem.*, 2009, **33**, 1224–1230. (c) L. F. Chibotaru, L. Ungur, C. Aronica, H. Elmoll, G. Pilet and D. Luneau, *J. Am. Chem. Soc.*, 2008, **130**, 12445–12455.

S44 F. Neese, ORCA–*an ab initio, density functional and semiempirical program package*, Version 4.2; Max-Planck institute for bioinorganic chemistry: Mülheim an der Ruhr, Germany, 2019.

S45 B. A. Hess, C. M. Marian, U. Wahlgren and O. Gropen, *Chem. Phys. Lett*. 1996, **251**, 365-371.

S46 C. Angeli, R. Cimiraglia, S. Evangelisti, T. Leininger and J. P. Malrieu, *J. Chem. Phys.*, 2001, **114**, 10252–10264.

S47 C. Angeli, R. Cimiraglia and J.-P. Malrieu, *Chem. Phys. Lett.*, 2001, **350**, 297–305.

S48 C. Angeli and R. Cimiraglia, *Theor. Chem. Acc.*, 2002, **107**, 313–317.

S49 C. Angeli, R. Cimiraglia and J.-P. Malrieu, *J. Chem. Phys.*, 2002, **17**, 9138–9153.

S50 A. Schafer, C. Huber and R. Ahlrichs, *J. Chem. Phys.*, 1994, **100**, 5829–5835.

S51 A. Schafer, H. Horn and R. Ahlrichs, *J. Chem. Phys.*, 1992, **97**, 2571–2577.

S52 F. Weigend and R. Ahlrichs, *Phys. Chem. Chem. Phys.*, 2005, **7**, 3297–3305.

S53 M. Atanasov, D. Ganyushin, K. Sivalingam and F. Neese, *Struct. Bond.*, 2012, **143**, 149–220.

S54 S. K. Singh, J. Eng, M. Atanasov and F. Neese, *Coord. Chem. Rev.*, 2017, **344**, 2–25.